Cellular and Molecular Life Sciences (2024) 81:228
https://doi.org/10.1007/s00018-024-05257-5

Cellular and Molecular Life Sciences

ORIGINAL ARTICLE

Cardiac-specific PFKFB3 overexpression prevents diabetic cardiomyopathy via enhancing OPA1 stabilization mediated by K6-linked ubiquitination

Jinlan Luo[1,2] · Shuiqing Hu[2] · Jingrui Liu[2] · Lili Shi[1] · Liman Luo[1] · Wenhua Li[1] · Yueting Cai[2] · Jiaxin Tang[1] · Siyang Liu[1] · Menglu Fu[1] · Ruolan Dong[3] · Yan Yang[4] · Ling Tu[1,5] · Xizhen Xu[2,5]

Received: 9 January 2024 / Revised: 1 April 2024 / Accepted: 27 April 2024
© The Author(s) 2024

Abstract

Diabetic cardiomyopathy (DCM) is a prevalent complication of type 2 diabetes (T2D). 6-phosphofructo-2-kinase/fructose-2,6-biphosphatase 3 (PFKFB3) is a glycolysis regulator. However, the potential effects of PFKFB3 in the DCM remain unclear. In comparison to db/m mice, PFKFB3 levels decreased in the hearts of db/db mice. Cardiac-specific PFKFB3 overexpression inhibited myocardial oxidative stress and cardiomyocyte apoptosis, suppressed mitochondrial fragmentation, and partly restored mitochondrial function in db/db mice. Moreover, PFKFB3 overexpression stimulated glycolysis. Interestingly, based on the inhibition of glycolysis, PFKFB3 overexpression still suppressed oxidative stress and apoptosis of cardiomyocytes in vitro, which indicated that PFKFB3 overexpression could alleviate DCM independent of glycolysis. Using mass spectrometry combined with co-immunoprecipitation, we identified optic atrophy 1 (OPA1) interacting with PFKFB3. In db/db mice, the knockdown of OPA1 receded the effects of PFKFB3 overexpression in alleviating cardiac remodeling and dysfunction. Mechanistically, PFKFB3 stabilized OPA1 expression by promoting E3 ligase NEDD4L-mediated atypical K6-linked polyubiquitination and thus prevented the degradation of OPA1 by the proteasomal pathway. Our study indicates that PFKFB3/OPA1 could be potential therapeutic targets for DCM.

✉ Ling Tu
lingtu@tjh.tjmu.edu.cn

✉ Xizhen Xu
xzxu@tjh.tjmu.edu.cn

[1] Department of Geriatric Medicine, Tongji Hospital, Tongji Medical College, Huazhong University of Science and Technology, Wuhan 430030, China

[2] Division of Cardiology and Department of Internal Medicine, Tongji Hospital, Tongji Medical College, Huazhong University of Science and Technology, Wuhan 430030, China

[3] Institute of Integrated Traditional Chinese and Western Medicine, Tongji Hospital, Tongji Medical College, Huazhong University of Science and Technology, Wuhan 430030, China

[4] Health Management Center, Tongji Hospital, Tongji Medical College, Huazhong University of Science and Technology, Wuhan 430030, China

[5] Hubei Key Laboratory of Genetics and Molecular Mechanisms of Cardiological Disorders, Wuhan 430030, China

Published online: 22 May 2024

Graphical Abstract

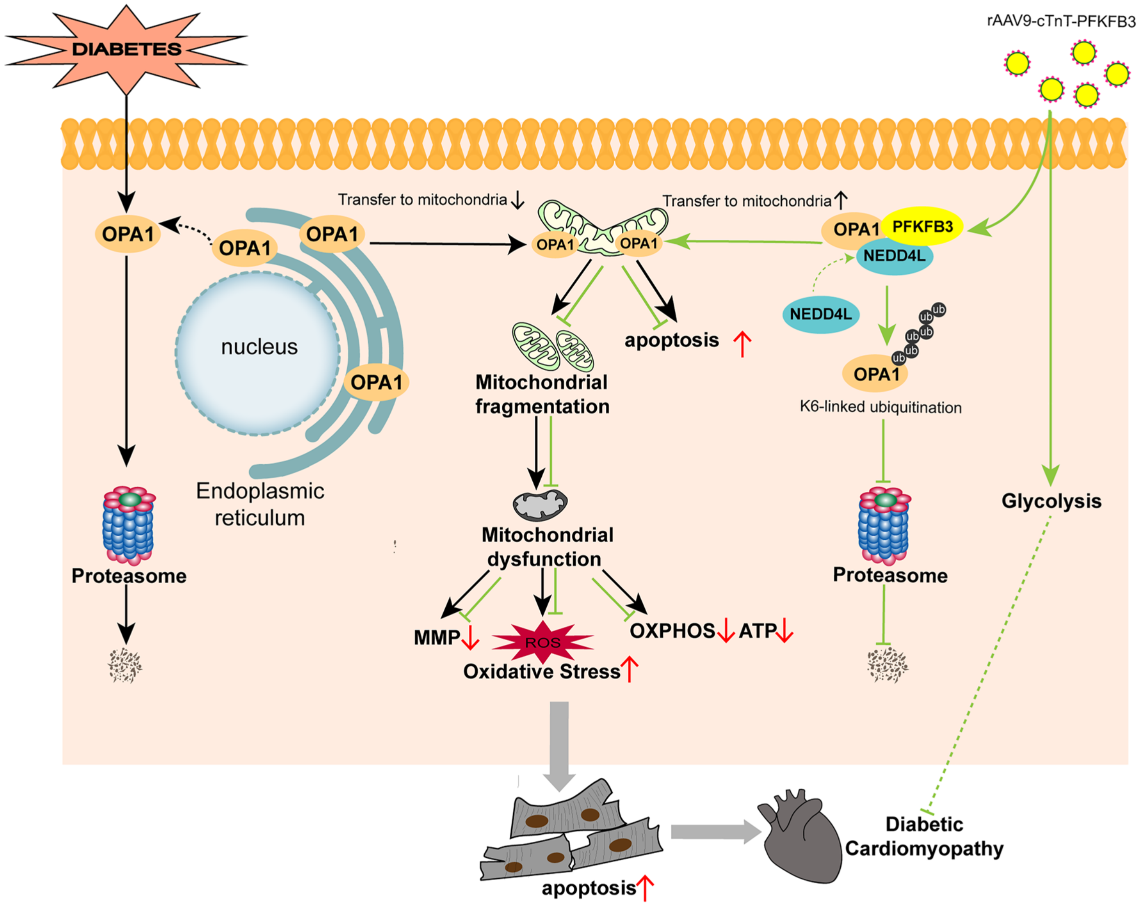
DIABETES
rAAV9-cTnT-PFKFB3
OPA1
OPA1
OPA1
nucleus
OPA1
Endoplasmic reticulum
Transfer to mitochondria ↓
OPA1
OPA1
Transfer to mitochondria ↑
OPA1
PFKFB3
NEDD4L
NEDD4L
ub
OPA1
K6-linked ubiquitination
Mitochondrial fragmentation
apoptosis ↑
Mitochondrial dysfunction
MMP↓
ROS
Oxidative Stress↑
OXPHOS↓ ATP↓
Proteasome
Proteasome
Glycolysis
apoptosis↑
Diabetic Cardiomyopathy

Keywords Heart failure · Mitochondrial dysfunction · Protein–protein interactions · rAAV9 · Therapeutics

Abbreviations

ATP	Adenosine triphosphate
AAV9	Adeno-associated virus serotype 9
Co-IP	Co-immunoprecipitation
CQ	Chloroquine
CHX	Cycloheximide
DCM	Diabetic cardiomyopathy
MMP	Mitochondrial membrane potential
MS	Mass spectrometry
OCR	Oxygen consumption rate
OXPHOS	Oxidative phosphorylation
OPA1	Optic atrophy 1
ECAR	Extracellular acidification rate
PFKFB3	6-Phosphofructo-2-kinase/fructose-2,6-biphosphatase 3
HF	Heart failure
ROS	Reactive oxygen species
TUNEL	Terminal-deoxynucleotidyl transferase-mediated nick end labeling
DHE	Dihydroethidium
WGA	Wheat Germ Agglutinin
TEM	Transmission electron microscopy

Introduction

Diabetes Mellitus (DM) has become "a pandemic of unprecedented magnitude," now affecting more than 537 million adults [1]. Cardiovascular disease is a common complication in diabetic patients, causing substantial morbidity and mortality and imposing a significant burden on society [2]. "Diabetic cardiomyopathy" (DCM), defined as impairments in cardiac structure and function without overt hypertension, coronary artery disease (CAD), or valvular disease, has been increasingly regarded as a unique entity since its first definition in 1972 by Rubler et al. [3, 4]. DCM is mainly characterized by left ventricular enlargement, myocardial hypertrophy, myocardial interstitial fibrosis and cardiac systolic and/or diastolic dysfunction, eventually leading to heart failure (HF) [5]. Indeed, traditional glucose-lowering therapy failed to improve cardiac function or reduce the risk of HF, while current routine HF treatment is similar whether or not the patient has DM. Although the emergence of sodium–glucose cotransporter 2 inhibitors (SGLT2i) [6] and glucagon-like peptide 1 receptor antagonists (GLP-1RA) [7] offers some promise in this field, the prevalence of HF in diabetic individuals is still as high as 22%, and the incidence is still rising [8]. Therefore, exploring effective therapeutic strategies for DCM is still the focus of current research.

Mitochondrial dysfunction is implicated as a critical pathogenesis of DCM [9]. The heart is a highly energy-demanding tissue and mitochondria are considered as the “powerhouse” due to their role in providing ATP through oxidative phosphorylation (OXPHOS). Furthermore, mitochondria play an important part in several cellular processes, such as reactive oxygen species (ROS) mediated signaling pathways [10], cytoplasmic calcium homeostasis [11] and apoptosis [12]. Accumulating evidence suggests that mitochondrial dysfunction, characterized by reduced ATP production, impaired oxidative-respiratory chain function, increased ROS production and cardiomyocyte apoptosis participates in the progression of DCM [13, 14]. Hence, focusing on mitochondrial dysfunction may hold promise for preventing DCM.

PFKFB3, also termed 6-phosphofructo-2-kinase/fructose-2,6-biphosphatase 3, assumes a critical function in the generation of stable cytoplasmic concentrations of fructose-2,6-bisphosphate (F-2,6-BP) in glycolysis. This metabolite serves as a preeminent allosteric activator, significantly augmenting the activity of the pivotal regulatory enzyme of glycolysis, phosphofructokinase-1 (PFK-1) [15]. Upregulating the expression of PFKFB3 has been shown to alleviate ROS

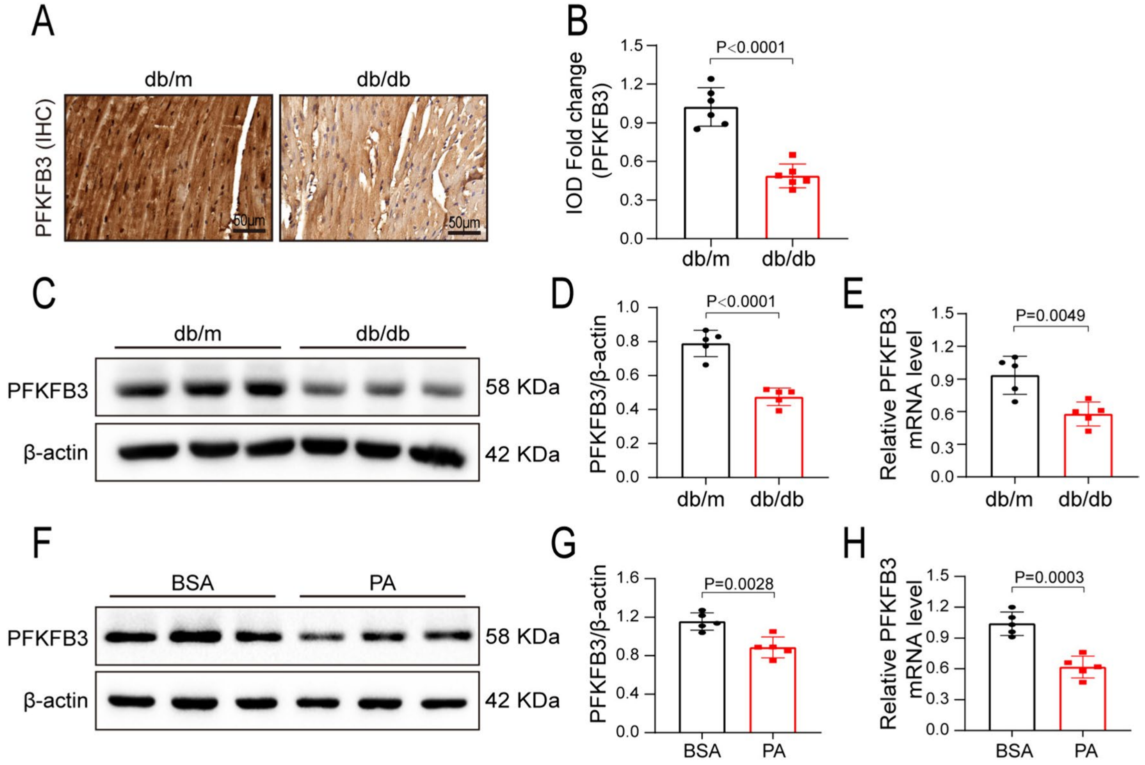

Fig. 1 Characterization of PFKFB3 expression in the cardiac tissues and cardiomyocytes. **A** and **B** Representative immunohistochemical staining and quantitative analysis of PFKFB3 expression in the hearts of db/db mice and db/m mice at 20 weeks. IOD, integrated optical density. **C**, **D** Representative Western blot and quantitative analysis of PFKFB3 expression in hearts of 20-week-old db/db mice and db/m mice. **E** The rt-qPCR analysis of PFKFB3 mRNA expression in hearts of 20-week-old db/db mice and db/m mice. n = 5–6/group. **F** and **G** Representative Western blot and quantitation analysis of PFKFB3 expression in AC16 cells treated with BSA or PA for 48 h. **H** The rt-qPCR analysis of PFKFB3 in AC16 cells treated with BSA or PA for 48 h. n = 5/group. Data are expressed as mean ± standard deviation (SD). $p < 0.05$ was considered significant

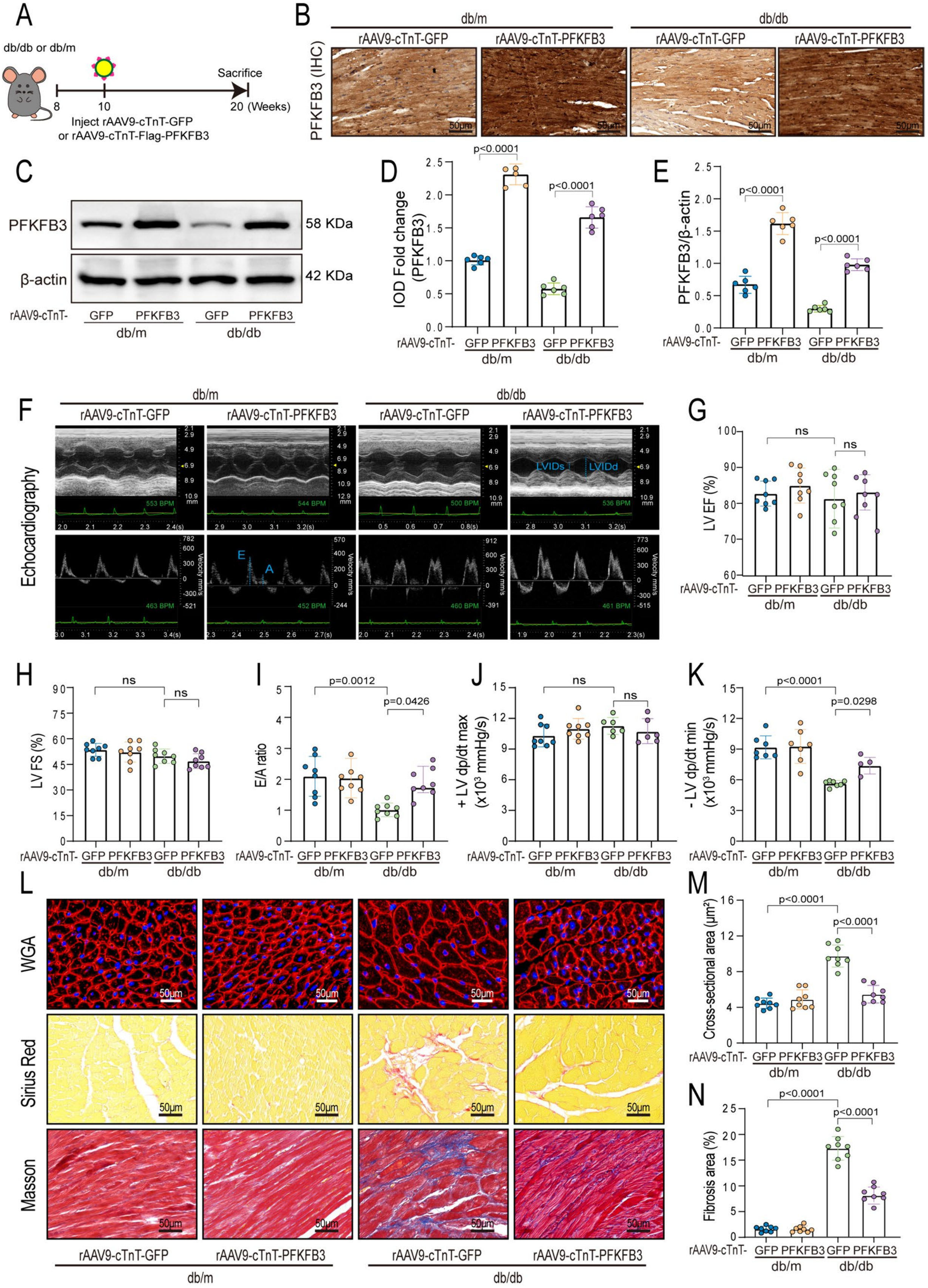
A
db/db or db/m
8
10
Sacrifice
20 (Weeks)
Inject rAAV9-cTnT-GFP
or rAAV9-cTnT-Flag-PFKFB3
B
db/m
db/db
rAAV9-cTnT-GFP
rAAV9-cTnT-PFKFB3
PFKFB3 (IHC)
50μm
C
PFKFB3
58 KDa
β-actin
42 KDa
rAAV9-cTnT- GFP PFKFB3 GFP PFKFB3
db/m db/db
D
IOD Fold change (PFKFB3)
p<0.0001
p<0.0001
E
PFKFB3/β-actin
p<0.0001
p<0.0001
F
Echocardiography
LVIDs
LVIDd
E
A
553 BPM
544 BPM
500 BPM
536 BPM
463 BPM
452 BPM
460 BPM
461 BPM
Velocity mm/s
G
LV EF (%)
ns
ns
H
LV FS (%)
ns
ns
I
E/A ratio
p=0.0012
p=0.0426
J
+ LV dp/dt max ($x10^3$ mmHg/s)
ns
ns
K
- LV dp/dt min ($x10^3$ mmHg/s)
p<0.0001
p=0.0298
L
WGA
Sirius Red
Masson
50μm
rAAV9-cTnT-GFP
rAAV9-cTnT-PFKFB3
db/m
db/db
M
Cross-sectional area (μm^2)
p<0.0001
p<0.0001
N
Fibrosis area (%)
p<0.0001
p<0.0001
rAAV9-cTnT- GFP PFKFB3 GFP PFKFB3
db/m db/db

◂**Fig. 2** Cardiac-specific overexpression of PFKFB3 alleviated cardiac dysfunction and myocardial remodeling in db/db mice. **A** Schematic diagram. The rAAV9-cTnT-GFP or rAAV9-cTnT-Flag-PFKFB3 were injected via the mice's tail vein in a volume of 150 µL (5*10^12 vg/mL). **B**, **D.** Representative immunohistochemical staining and quantitative analysis of PFKFB3 in the hearts of db/m and db/db mice. Scale bars, 50 µm. **C**, **E**. Western blot and quantitative analysis of PFKFB3 expression in hearts of db/db and db/m mice. **F** Representative echocardiography images in db/m and db/db mice; LVID: left ventricular internal dimension; s: end-systole; d: end-diastole. **G**–**I** LVEF (left ventricular ejection fraction), LVFS (left ventricular fractional shortening), E/A ratio (the ratio of E wave to A wave). **J**, **K** Hemodynamics analysis of the maximal and minimal first derivative of LV pressure. The heart rate is reliably within the 450–500 bpm range. **L.** Representative images of wheat germ agglutinin (WGA) staining, Sirius Red staining and Masson staining. Scale bars, 50 µm. **M** Quantitative analysis of cardiomyocyte sizes based on WGA staining. **N** Quantitative analysis of fibrosis percentage based on Masson staining. n = 6–8/group. Data are expressed as mean ± SD. $p < 0.05$ was considered significant

accumulation and mitochondria dysfunction in human proximal tubular epithelial cells (PTECs), thereby attenuating kidney injury [16]. However, whether PFKFB3 is involved in DCM remains unclear. This study aims to explore the potential effects of PFKFB3 in DCM and the molecular mechanisms involved.

Methods

Animals and ethical approval

8-week-old male leptin receptor-deficient (C57BLKS/J-LepRdb/LepRdb, db/db) mice and their control littermates (C57BLKS/J-LepRdb/+, db/m) were fed under controlled conditions (12-h light/dark cycle, 22 ± 1℃, and 50 ± 10% humidity), with standard chow and water provided ad libitum.

Statistical analysis

The data is presented as mean ± SD, and statistical analysis was carried out using an unpaired Student's t-test to compare the two groups. We employed one-way ANOVA for multiple groups, followed by Tukey's post hoc analysis. All analyses were performed with GraphPad Prism version 8.0.2 (GraphPad Software, La Jolla, CA). Statistical significance was expressed as $p < 0.05$.

Extended information about the Materials and Methods can be accessed in the Supplementary Materials.

Results

Characterization of PFKFB3 expression in the cardiac tissues and cardiomyocytes

We assessed the expression of PFKFB3 in the hearts of db/db and db/m mice. Immunohistochemical staining and Western blot analysis revealed that PFKFB3 expression was considerably reduced in the myocardial tissue of db/db mice compared to db/m mice (Fig. 1A–D). PFKFB3 mRNA level was also reduced in the hearts of db/db animals (Fig. 1E). We also assessed the expression of PFKFB2 in the cardiac tissue. It is an isoenzyme of PFKFB3, while other isoenzymes, such as PFKFB1 and PFKFB4, are not expressed in the heart [17]. The expression of PFKFB2 remained unaltered in the hearts of db/db mice as compared to db/m mice (Fig. S1A, S1B). In vitro, the AC16 human cardiomyocyte cell line was treated with saturated PA (Palmitate acid, 200 µM) or BSA (Bovine serum albumin, solvent control, 10%) for 48 h as previously described [18, 19]. PFKFB3 expression in the protein and mRNA levels was decreased under PA treatment (Fig. 1F–H). These data demonstrated that myocardial PFKFB3 expression was decreased in db/db mice, suggesting a potential involvement in the development of DCM.

Cardiac-specific overexpression of PFKFB3 alleviated cardiac dysfunction and myocardial remodeling in db/db mice

In a prior study, recombinant adeno-associated virus 9 (rAAV9)-mediated gene expression, guided by the cTnT (cardiomyocyte-specific troponin T) promoter, exhibited remarkable cardiac tissue affinity, surpassing the liver by 640-fold [20]. In exploring PFKFB3 overexpression's potential effects on DCM, Ten-week-old mice were injected either with rAAV9-cTnT-flag-PFKFB3 or rAAV9-cTnT-GFP (Fig. 2A). After ten weeks, PFKFB3 was successfully overexpressed in the myocardial tissue of the mice (Fig. 2B–E). In comparison to db/m + rAAV9-cTnT-GFP mice, db/db + rAAV9-cTnT-GFP mice exhibited significant increases in body weight, fasting blood glucose levels, serum total cholesterol (TC) levels, and high-density lipoprotein (HDL) cholesterol levels (Table 1 and Fig. S2A, S2B). Additionally, the db/db + rAAV9-cTnT-GFP mice exhibited impaired glucose tolerance and reduced insulin sensitivity, as verified by the glucose tolerance test (GTT) and insulin tolerance test (ITT) (Fig. S2C–S2F). However, PFKFB3 overexpression had no significant effects on body weight, fasting blood glucose, blood lipids, impaired glucose

Table 1 Blood lipids characteristics in db/m and db/db mice with different adeno-associated virus interventions

Parameter/Group	db/m		db/db	
	rAAV-GFP	rAAV-PFKFB3	rAAV-GFP	rAAV-PFKFB3
Body weight (g)	27.45 ± 2.36	27.98 ± 1.77	61.04 ± 4.47*	61.29 ± 5.10
TC (mmol/L)	2.12 ± 0.24	1.93 ± 0.25	3.39 ± 0.83*	4.00 ± 0.74
TG (mmol/L)	1.01 ± 0.31	1.14 ± 0.32	1.02 ± 0.43	0.70 ± 0.12
LDL (mmol/L)	0.22 ± 0.13	0.25 ± 0.07	0.19 ± 0.07	0.19 ± 0.09
HDL (mmol/L)	1.14 ± 0.14	0.95 ± 0.20	1.57 ± 0.41*	1.76 ± 0.52

TG Triglyceride, *TC* total cholesterol, *HDL* high-density lipoprotein, *LDL* low-density lipoprotein

n = 8/group, Data are presented as mean ± SD. *$p < 0.05$ versus db/m + rAAV9-cTnT-GFP

Table 2 Echocardiographic characteristics in db/m and db/db mice with different adeno-associated virus interventions

Parameter/Group	db/m		db/db	
	rAAV-GFP	rAAV-PFKFB3	rAAV-GFP	rAAV-PFKFB3
E/A	2.14 ± 0.62	2.08 ± 0.61	1.04 ± 0.21*	1.77 ± 0.41#
LVEF (%)	81.38 ± 3.02	83.44 ± 4.24	80.04 ± 7.11	81.71 ± 4.29
LVFS (%)	54.08 ± 3.57	51.53 ± 6.13	50.34 ± 3.97	49.92 ± 8.45
SV (μL)	31.08 ± 1.99	31.54 ± 5.25	31.35 ± 4.67	31.59 ± 5.83
HR (b.p.m)	523 ± 49	534 ± 33	527 ± 42	511 ± 26
CO (mL/min)	17.49 ± 1.38	17.80 ± 2.36	20.80 ± 5.01	17.02 ± 8.12
LV Mass (mg)	133.06 ± 21.06	133.57 ± 22.18	168.01 ± 9.55*	136.93 ± 23.71#
LVAW; s (mm)	1.74 ± 0.12	1.75 ± 0.16	1.80 ± 0.25	1.75 ± 0.19
LVAW; d (mm)	1.09 ± 0.14	1.02 ± 0.22	1.12 ± 0.19	1.03 ± 0.24
LVPW; s (mm)	1.59 ± 0.26	1.61 ± 0.28	1.58 ± 0.35	1.63 ± 0.14
LVPW; d (mm)	1.09 ± 0.18	1.17 ± 0.26	1.06 ± 0.39	1.11 ± 0.22
LVID; s (mm)	1.19 ± 0.30	1.15 ± 0.26	1.27 ± 0.58	1.17 ± 0.33
LVID; d (mm)	2.92 ± 0.24	2.86 ± 0.30	3.25 ± 0.29	2.79 ± 0.54

E/A ratio of E wave to A wave, *LVEF* left ventricle ejection fraction, *LV*FS left ventricle fractional shortening, *SV* stroke volume, *HR* heart rate, CO cardiac output, *LV Mass* left ventricle mass, *LVAW,*s left ventricular anterior wall thickness at end-systole, *LVAW,d* left ventricular anterior wall thickness at end-diastole, *LVPW,s* left ventricular posterior wall thickness at end-systole, *LVPW,d* left ventricular posterior wall thickness at end-diastole, *LVID,s* left ventricular internal-systolic dimension, *LVID,d* left ventricular internal-diastolic dimension. n = 8/group

Data are presented as mean ± SD, *$p < 0.05$ versus db/m + rAAV9-cTnT-GFP, #$p < 0.05$ versus db/db + rAAV9-cTnT-GFP

tolerance, and declined insulin sensitivity in db/db mice. These data indicate that cardiac-specific overexpression of PFKFB3 had no discernible effects on the glycolipid metabolic disorder in db/db mice.

Echocardiography and Millar catheter were utilized to assess cardiac function and hemodynamic parameters. No significant alterations in fractional shortening (FS), ejection fraction (EF) and + LV dp/dt max (maximal first derivative of left ventricular pressure over time; a measure of cardiac contractility) between the db/m + rAAV9-cTnT-GFP and the db/db + rAAV9-cTnT-GFP mice (Fig. 2F–H, J). The E/A ratio (the ratio of early (E-wave) to late (A-wave) mitral inflow velocity) and -LV dp/dt min (minimal first derivative of left ventricular pressure over time; a measure of cardiac relaxation) were decreased in the db/db + rAAV9-cTnT-GFP mice compared to the db/m + rAAV9-cTnT-GFP mice, but reversed by PFKFB3 overexpression (Fig. 2F, I, K). Cardiac hypertrophy and interstitial fibrosis are pivotal alterations in DCM. Compared with db/m + rAAV9-cTnT-GFP mice, left ventricular mass was increased in db/db + rAAV9-cTnT-GFP mice, which was mitigated by PFKFB3 overexpression (Table 2). Additionally, db/db + rAAV9-cTnT-GFP mice displayed evident cardiac remodeling, characterized by enlarged cardiomyocyte cross-sectional areas and heightened interstitial collagen deposition within the myocardium, which was alleviated by PFKFB3 overexpression (Fig. 2L–N). In conclusion, cardiac-specific overexpression of PFKFB3 significantly improved cardiac function and attenuated myocardial remodeling in db/db mice.

Cardiac-specific overexpression of PFKFB3 inhibited myocardial oxidative stress and apoptosis

Previous evidence suggests that increased oxidative stress and cardiomyocyte apoptosis are prevalent characteristics of DCM [21, 22]. As expected, the apoptosis rate determined by TUNEL staining (Fig. 3A, C) and the levels of apoptosis-related proteins, including Bax and Cleaved caspase-3, were elevated in myocardial tissues of db/db + rAAV9-cTnT-GFP mice compared to db/m + rAAV9-cTnT-GFP mice (Fig. 3D, E). In contrast, the level of the anti-apoptosis protein Bcl-2 was lower in db/db + rAAV9-cTnT-GFP mice (Fig. 3D, E). Additionally, the amount of myocardial superoxide anion was increased in db/db + rAAV9-cTnT-GFP mice compared to that in the db/m + rAAV9-cTnT-GFP group, as determined by dihydroethidium (DHE) staining (Fig. 3A, B). In db/db mice, the overexpression of PFKFB3 in the myocardium led to a significant reduction in cardiomyocyte apoptosis and oxidative stress (Fig. 3A–E).

In vitro, we transfected AC16 cells with pcDNA3.1 or pcDNA3.1-Flag-PFKFB3 plasmids. The overexpression of PFKFB3 significantly reduced apoptosis in PA-treated AC16 cells, as evidenced by the decrease in the percentage of apoptotic cells (Fig. S3A, S3D), the decreased expression of Bax and Cleaved caspase-3 coupled with elevated levels of Bcl-2 (Fig. S3C, S3F). Similarly, flow cytometry analysis revealed that PFKFB3 overexpression significantly decreased ROS levels induced by PA in AC16 cells (Fig. S3B, S3E). In summary, cardiac-specific overexpression of PFKFB3 significantly inhibited myocardial oxidative stress and apoptosis in DCM.

Cardiac-specific overexpression of PFKFB3 reduced mitochondrial fragmentation and partially restored mitochondrial function

Impaired mitochondrial function increases ROS production and apoptosis in cardiovascular disease [23]. Abnormal-shaped mitochondria, characterized by a reduction of the mean size, were observed in myocardial samples from db/db + rAAV9-cTnT-GFP mice compared to db/m + rAAV9-cTnT-GFP mice using transmission electron microscopy (TEM) (Fig. 3F and G). Additionally, a substantial loss of electron density and decreased mitochondrial cristae, accompanied by an increased proportion of ruptured and disorganized cristae, were observed in diabetic hearts compared to control mice (Fig. 3F, H, I). Similarly, MitoTracker staining of PA-treated AC16 cells revealed mitochondrial fragmentation (Fig. S4A and S4B). However, PFKFB3 overexpression promoted mitochondrial fusion, as evidenced by increased mitochondrial size in the hearts of db/db mice and partially recovery of the mitochondrial network in PA-treated AC16 cells (Figs. 3F and G, S4A and S4B). The mitochondrial membrane potential (MMP) was measured using the JC-1 dye and a flow cytometer. The ratio of monomers that produced green fluorescence indicated the degree of mitochondrial depolarization. PA treatment triggered heightened mitochondrial depolarization, resulting in a reduction in MMP, which was inhibited by PFKFB3 overexpression (Fig. S4C and S4D).

Since the mitochondria serve as the epicenters of OXPHOS and ATP synthesis in mammalian cells, we scrutinized mitochondrial respiratory capacity by assessing mitochondrial oxygen consumption rate (OCR) and ATP levels. As predicted, PA treatment significantly reduced mitochondrial respiratory capacity, including basal respiration, ATP-related respiration, and maximal respiration, compared to pcDNA3.1-treated AC16 cells (Fig. S4E and S4F). Concurrently, ATP levels were decreased in the hearts of db/db + rAAV9-cTnT-GFP mice compared to db/m + rAAV9-cTnT-GFP mice (Fig. 3J). Remarkably, PFKFB3 overexpression significantly enhanced mitochondrial respiration and increased ATP levels (Figs. 3J and S4E and S4F). Moreover, we assessed the level of mitochondrial biogenesis-related protein PGC-1α and the mitochondrial respiratory chain complexes I–V, designated as CI-NDUFS1, CII-SDHA, CIII-UQCRC2, CIV-MTCO2, and CV-ATP5A1. The presence of the Flag validated the efficiency of PFKFB3 overexpression (Fig. 3K). There were no noteworthy distinctions in PGC-1α and mitochondrial complexes II, III, and IV across the experimental groups. However, in the hearts of db/db + rAAV9-cTnT-GFP mice, the expression of mitochondrial complexes I and V was markedly decreased, which was partially recovered by PFKFB3 overexpression (Fig. 3K and L). The findings highlight the crucial role of PFKFB3 overexpression in preserving mitochondrial integrity and alleviating mitochondrial dysfunction in db/db myocardial tissue.

Impaired glycolysis has been observed in the cardiac tissues of both diabetic individuals and experimental diabetic animals [24], and several studies have reported that restoring glycolytic metabolism alleviated DCM [25–27]. PFKFB3 is a regulator of glycolytic activity [28–30]. Li et al. discovered that elevating SIRT3 levels relieves DCM by upregulating the expression of PFKFB3, thereby enhancing glycolytic processes. So, we analyzed lactic acid levels (a product of glycolysis) in the cardiac tissues of mice and assessed the extracellular acidification rate (ECAR) in AC16 cells. As expected, PFKFB3 overexpression resulted in elevated lactic acid levels in the hearts of both db/m and db/db mice (Fig. S5A). In AC16 cells, PFKFB3 overexpression increased baseline ECAR, glycolysis, and glycolytic

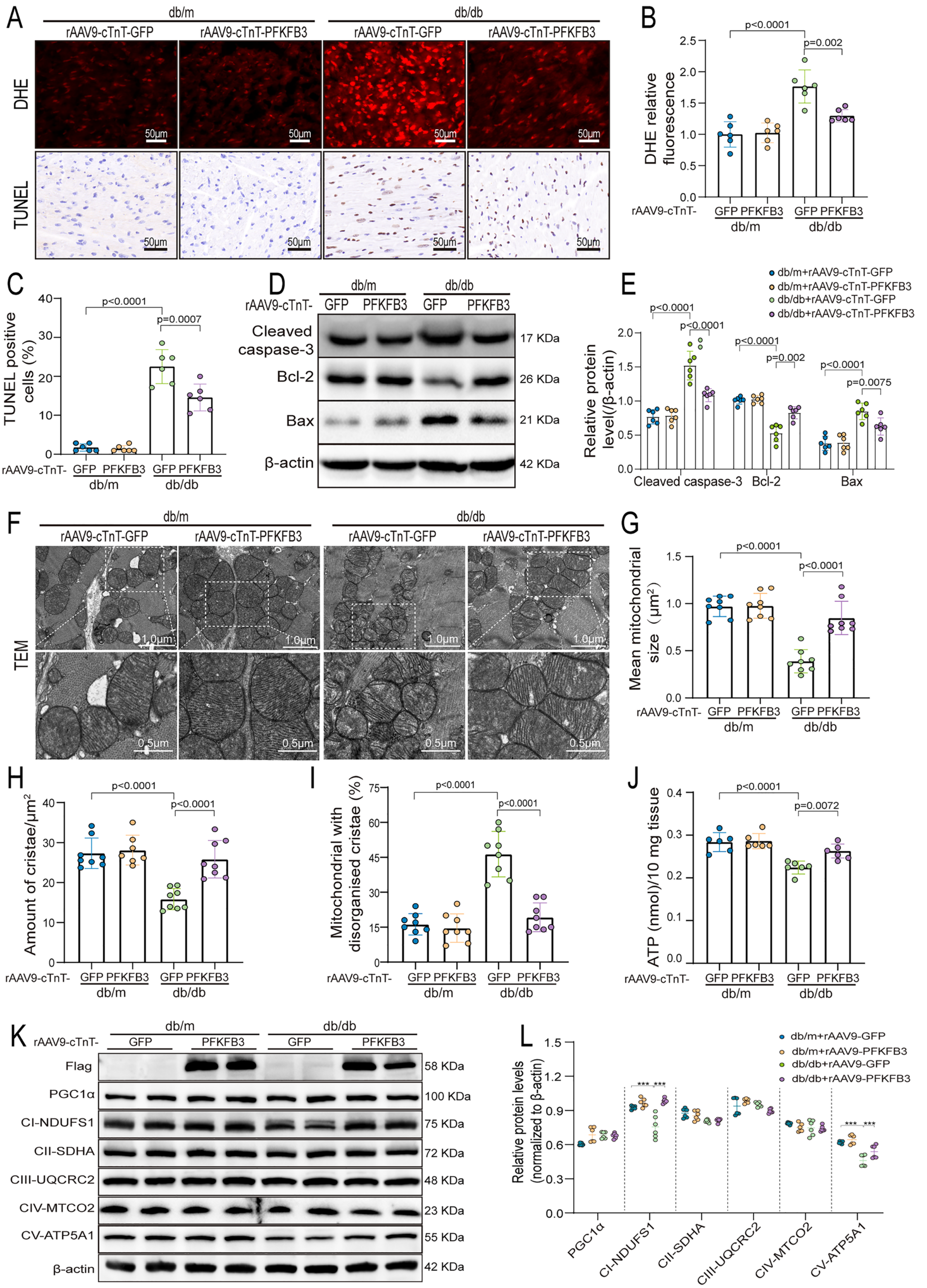
A
db/m
db/db
rAAV9-cTnT-GFP
rAAV9-cTnT-PFKFB3
rAAV9-cTnT-GFP
rAAV9-cTnT-PFKFB3
DHE
TUNEL
50μm
B
DHE relative fluorescence
p<0.0001
p=0.002
2.5
2.0
1.5
1.0
0.5
0.0
rAAV9-cTnT-
GFP PFKFB3
db/m
GFP PFKFB3
db/db
C
TUNEL positive cells (%)
p<0.0001
p=0.0007
40
30
20
10
0
D
db/m
db/db
rAAV9-cTnT-
GFP PFKFB3 GFP PFKFB3
Cleaved caspase-3
Bcl-2
Bax
β-actin
17 KDa
26 KDa
21 KDa
42 KDa
E
db/m+rAAV9-cTnT-GFP
db/m+rAAV9-cTnT-PFKFB3
db/db+rAAV9-cTnT-GFP
db/db+rAAV9-cTnT-PFKFB3
Relative protein level(/β-actin)
p<0.0001
p<0.0001
p<0.0001
p=0.002
p<0.0001
p=0.0075
2.0
1.5
1.0
0.5
0.0
Cleaved caspase-3
Bcl-2
Bax
F
db/m
db/db
rAAV9-cTnT-GFP
rAAV9-cTnT-PFKFB3
rAAV9-cTnT-GFP
rAAV9-cTnT-PFKFB3
TEM
1.0μm
0.5μm
G
Mean mitochondrial size (μm²)
p<0.0001
p<0.0001
1.5
1.0
0.5
0.0
H
Amount of cristae/μm²
p<0.0001
p<0.0001
40
30
20
10
0
I
Mitochondrial with disorganised cristae (%)
p<0.0001
p<0.0001
75
60
45
30
15
0
J
ATP (nmol)/10 mg tissue
p<0.0001
p=0.0072
0.4
0.3
0.2
0.1
0.0
K
rAAV9-cTnT-
db/m
db/db
GFP
PFKFB3
GFP
PFKFB3
Flag
PGC1α
CI-NDUFS1
CII-SDHA
CIII-UQCRC2
CIV-MTCO2
CV-ATP5A1
β-actin
58 KDa
100 KDa
75 KDa
72 KDa
48 KDa
23 KDa
55 KDa
42 KDa
L
db/m+rAAV9-GFP
db/m+rAAV9-PFKFB3
db/db+rAAV9-GFP
db/db+rAAV9-PFKFB3
Relative protein levels (normalized to β-actin)
***
***
***
***
1.5
1.2
0.9
0.6
0.3
0.0
PGC1α
CI-NDUFS1
CII-SDHA
CIII-UQCRC2
CIV-MTCO2
CV-ATP5A1

◂**Fig. 3** Cardiac-specific overexpression of PFKFB3 inhibited myocardial oxidative stress, apoptosis, mitochondrial fragmentation and dysfunction in db/db mice. **A** Representative DHE and TUNEL staining images. Scale bars, 50 µm. **B** Quantitative analysis of DHE relative fluorescence. **C** Quantitative data of the TUNEL positive cells. **D**, **E** Representative Western blot of Cleaved caspase-3, Bax, Bcl-2 and associated quantitation analysis. **F** Representative transmission electron microscopic images of mitochondria. Scale bars, 1.0 µm, 0.5 µm. **G** Quantitative analysis of mean mitochondrial size. **H** The cristae number. **I** The proportion of mitochondria with disorganized cristae. **J** Quantification of ATP levels per 10 mg cardiac tissue. **K**, **L** Representative Western blot and quantitative analysis of Flag, PGC-1α and mitochondrial respiratory chain complex I–V (CI–CV). n = 6–8/group. Data are expressed as mean ± SD. $p < 0.05$ was considered significant

capacity, regardless of PA intervention (Fig. S5B, S5C). Consistent with Li's study, our results suggest that PFKFB3 overexpression stimulated glycolysis. 2-DG (2-deoxyglucose, a hexokinase 2 inhibitor) is a common glycolytic inhibitor that significantly inhibits the level of glycolysis (Fig. S5B). Interestingly, under the condition of inhibited glycolysis with 2-DG, overexpression of PFKFB3 still suppressed PA-induced oxidative stress and apoptosis, which indicates that PFKFB3 overexpression can alleviate DCM independent of glycolysis (Fig. S5D–S5G).

PFKFB3 interacts with OPA1

To investigate the mechanisms underlying the protective effects of PFKFB3 overexpression against DCM other than glycolysis, we employed mass spectrometry. AC16 cells were exposed to adenovirus-PFKFB3 (Ad-PFKFB3) or control vectors (Ad-GFP) for 12 h, followed by a 48-h treatment with PA. Subsequently, immunoprecipitation and immunoblotting analyses were performed, accompanied by Coomassie Blue Staining and liquid chromatography-tandem mass spectrometry (LC–MS/MS) (Fig. 4A, B). Next, we compared the 1387 potential copurified proteins with the 220 DCM-related proteins from DisGeNet (a database of human gene-disease associations) and the 428 mitochondrial dysfunction-related proteins from GeneCards (The Human Gene Database) (Fig. 4C). Only one potential binding protein, optic atrophy 1 (OPA1), was selected. The mass spectrogram of OPA1 is demonstrated in Fig. 4D. To validate the interaction between PFKFB3 and OPA1 in DCM, we conducted co-immunoprecipitation (Co-IP) assays using antibodies against PFKFB3 and OPA1 in the hearts of db/db mice (Fig. 4E). Additionally, we conducted immunofluorescence staining to visually demonstrate the colocalization of PFKFB3 and OPA1 in AC16 cells. The images revealed a robust colocalization between PFKFB3 and OPA1 (Fig. 4F).

By employing ZDOCK and the Prodigy server for protein–protein docking, we could anticipate the binding site and the affinity of PFKFB3 towards OPA1, calculated at −11.3 kcal/mol (Fig. 4G). To identify the specific binding motif of PFKFB3, we introduced two truncated mutations of PFKFB3, spanning amino acids 1–245 (P1) and 246–552 (P2). HEK293T cells were transfected with HA-OPA1 and either pcDNA3.1 or Flag-PFKFB3 1–245 (P1) or Flag-PFKFB3 246–552 (P2) or full-length Flag-PFKFB3 (P3), followed by Co-IP analysis. As indicated in Fig. 4H, both full-length Flag-PFKFB3 (P3) and Flag-PFKFB3 1–245 (P1) effectively immunoprecipitated with HA-OPA1, but Flag-PFKFB3 246–552 (P2) failed to immunoprecipitate with HA-OPA1. This implies that PFKFB3 interacted with OPA1 via its N-terminal domain (amino acids 1–245).

The interaction between PFKFB3 and OPA1 raises an intriguing question: Does PFKFB3 modulate OPA1? Our data reveal a significant reduction in OPA1 expression in the hearts of db/db mice compared to db/m mice. Notably, PFKFB3 overexpression partially restored OPA1 protein levels in the hearts of db/db mice, while mRNA levels of OPA1 remained unaffected (Fig. 4I–K). In vitro, OPA1 expression decreased in PA-treated AC16 cells. However, the transfection of AC16 cells with Flag-PFKFB3-encoding plasmids effectively rescued this decline in OPA1, increasing its protein levels in a dose-dependent manner (Fig. 4L–N). These data robustly indicate that PFKFB3 interacts with and regulates the protein levels of OPA1.

OPA1 knockdown attenuated the effects of PFKFB3 overexpression in alleviating cardiac dysfunction and remodeling in db/db mice

To uncover OPA1's pivotal role in mediating PFKFB3's protection against DCM, we utilized a cardiomyocyte-specific viral shRNA targeting OPA1, driven by the cTnT promoter (Fig. 5A). The procedure is outlined in Fig. 5B. Briefly, nine-week-old db/db mice received either rAAV9-cTnT-shOPA1 or rAAV9-cTnT-vector. One week later, these mice received injections with rAAV9-cTnT-Flag-PFKFB3 or rAAV9-cTnT-vector. Immunohistochemistry and Western blot confirmed OPA1 knockdown and PFKFB3 overexpression. rAAV9-cTnT-shOPA1 significantly reduced OPA1 expression while rAAV9-cTnT-flag-PFKFB3 markedly increased PFKFB3 levels in the myocardium of db/db mice (Fig. 5C, Fig. S6A–S6F). The echocardiographic and hemodynamic analysis demonstrated that cardiomyocyte-specific overexpression of PFKFB3 inhibited the decline in diastolic function, as evidenced by the elevated E/A ratio and -LV dp/dt min in diabetic hearts. However, the knockdown of OPA1 blocked the protective effects of PFKFB3 on diastolic

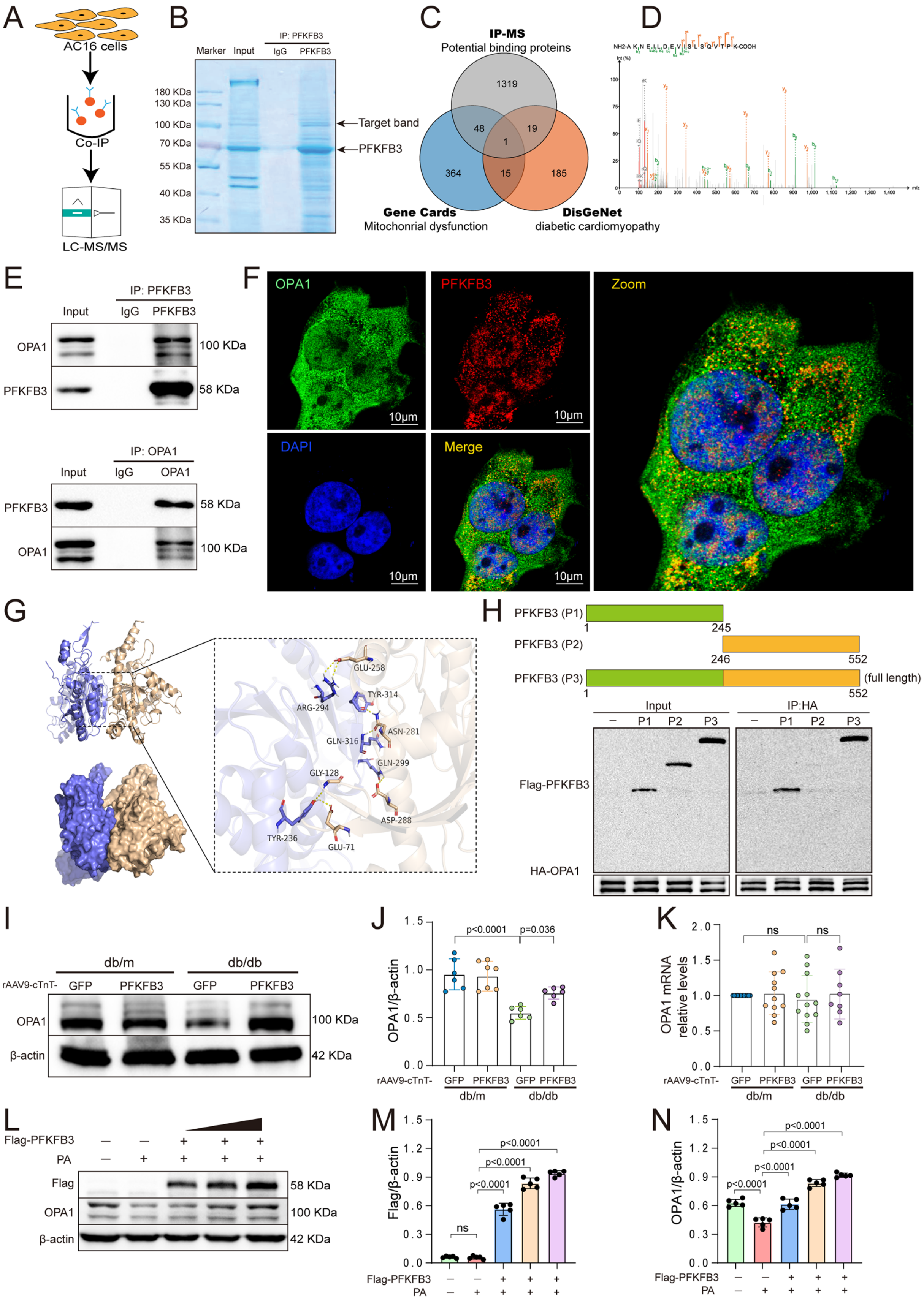
A
AC16 cells
Co-IP
LC-MS/MS
B
Marker
Input
IP: PFKFB3
IgG
PFKFB3
180 KDa
130 KDa
100 KDa
70 KDa
55 KDa
40 KDa
35 KDa
Target band
PFKFB3
C
IP-MS
Potential binding proteins
1319
48
19
1
364
15
185
Gene Cards
Mitochonrial dysfunction
DisGeNet
diabetic cardiomyopathy
D
E
IP: PFKFB3
Input
IgG
PFKFB3
OPA1
PFKFB3
100 KDa
58 KDa
IP: OPA1
Input
IgG
OPA1
PFKFB3
OPA1
58 KDa
100 KDa
F
OPA1
PFKFB3
Zoom
DAPI
Merge
10μm
G
GLU-258
ARG-294
TYR-314
ASN-281
GLN-316
GLN-299
GLY-128
ASP-288
TYR-236
GLU-71
H
PFKFB3 (P1)
1
245
PFKFB3 (P2)
246
552
PFKFB3 (P3)
(full length)
1
552
Input
IP:HA
–
P1
P2
P3
Flag-PFKFB3
HA-OPA1
I
db/m
db/db
rAAV9-cTnT-
GFP
PFKFB3
OPA1
β-actin
100 KDa
42 KDa
J
OPA1/β-actin
p<0.0001
p=0.036
1.5
1.0
0.5
0.0
rAAV9-cTnT-
GFP
PFKFB3
db/m
db/db
K
OPA1 mRNA relative levels
ns
ns
2.0
1.5
1.0
0.5
0.0
rAAV9-cTnT-
GFP
PFKFB3
db/m
db/db
L
Flag-PFKFB3
PA
Flag
OPA1
β-actin
58 KDa
100 KDa
42 KDa
M
Flag/β-actin
ns
p<0.0001
p<0.0001
p<0.0001
1.5
1.2
0.9
0.6
0.3
0.0
Flag-PFKFB3
PA
N
OPA1/β-actin
p<0.0001
p<0.0001
p<0.0001
p<0.0001
1.5
1.2
0.9
0.6
0.3
0.0
Flag-PFKFB3
PA

◂**Fig. 4** PFKFB3 interacts with OPA1. **A** Schematic diagram. **B** Coomassie Blue staining. **C** Venn diagram. **D** Mass spectrogram of OPA1. **E** Endogenous immunoprecipitation of PFKFB3 and OPA1 in cardiac tissue. **F** Immunofluorescence of PFKFB3 (red) and OPA1 (green) in AC16 cells, scale bars, 10 µm. **G** The interaction diagram of PFKFB3 protein and OPA1 protein shows that the wheat color is OPA1, the blue color is PFKFB3, and the yellow dotted line indicates hydrogen bonding. **H** Co-IP assay of PFKFB3 deletion mutants and HA-OPA1. HEK293T cells were co-transfected with HA-OPA1 and either pcDNA3.1 or Flag-PFKFB3 1–245(P1) or Flag-PFKFB3 246–552(P2) or Flag-PFKFB3 full-length (P3). **I**, **J** Representative Western blot and quantitative analysis of OPA1 expression in db/m and db/db mice. **K** The rt-qPCR analysis of OPA1 mRNA expression in db/m and db/db mice. **L–N** Representative Western blot and quantitative analysis of OPA1 and Flag expression under the treatment of PA and transfected with Flag-PFKFB3 plasmids in different doses. n = 6–8/group. Data are expressed as mean ± SD. $p < 0.05$ was considered significant

function in db/db mice (Fig. 5C–E). Moreover, PFKFB3 overexpression attenuated cardiac remodeling, including cardiomyocyte hypertrophy and myocardial interstitial fibrosis, while OPA1 knockdown in cardiomyocytes nullified PFKFB3's protective effects in diabetic hearts (Fig. 5C, F and G). Thus, cardiomyocyte-specific OPA1 knockdown significantly attenuated the beneficial impact of PFKFB3 on cardiac structure and function, underscoring the PFKFB3's protective effect against DCM depending on the presence of OPA1.

OPA1 knockdown attenuated the inhibitory effects of PFKFB3 overexpression on myocardial apoptosis and oxidative stress

OPA1 has been reported to protect cells from apoptosis and inhibit oxidative stress [31–33]. Therefore, we further explored whether PFKFB3 overexpression improves cardiomyocyte apoptosis and oxidative stress in db/db mice through OPA1. As anticipated, the TUNEL staining indicated that cardiomyocyte-specific overexpression of PFKFB3 significantly reduced the percentage of apoptotic cardiomyocytes (Fig. 6A and B). DHE staining demonstrated that PFKFB3 overexpression effectively inhibited the production of superoxide anion in diabetic hearts (Fig. 6A, C). However, specific knockdown of OPA1 in cardiomyocytes attenuated all the inhibitory effects of PFKFB3 on myocardial apoptosis and oxidative stress in diabetic hearts (Fig. 6A–C). Moreover, flow cytometry results revealed that transfection of Flag-PFKFB3 plasmids significantly alleviated apoptosis induced by PA and the production of ROS in vitro (Fig. S7A–S7D). To further validate whether the beneficial effects of PFKFB3 in anti-apoptosis and anti-oxidative stress depend on OPA1 in vitro, we designed a specific small interfering RNA (siRNA) to knock down the expression of OPA1. Consistent with in vivo findings, OPA1 knockdown using siRNA attenuated the inhibitory effects of PFKFB3 overexpression on PA-induced apoptosis and ROS production (Fig. S7A–S7D). In conclusion, PFKFB3 overexpression inhibited myocardial apoptosis and oxidative stress in db/db mice, dependent on OPA1 expression.

OPA1 knockdown attenuated the protective effects of PFKFB3 overexpression on mitochondrial morphology and function

Since OPA1 is an essential regulatory protein during mitochondrial fusion, we explored whether PFKFB3 overexpression regulates mitochondrial morphology and function through OPA1. TEM unveiled that PFKFB3 overexpression increased the mean size of mitochondria and the number of cristae, while reducing the number of disorganized cristae (Fig. 6A, D–F). Additionally, MitoTracker staining demonstrated that transfecting Flag-PFKFB3 inhibited the mitochondrial fragmentation induced by PA (Fig. S8A, S8C). However, OPA1 knockdown attenuated the beneficial effects of PFKFB3 overexpression on mitochondrial morphology and ultrastructure (Fig. 6A, D–F). In vitro, OPA1 knockdown using siRNA attenuated the protective effects of PFKFB3 overexpression on the mitochondrial network in AC16 cells treated with PA (Fig. S8A, S8C). Mitochondrial MMP, OXPHOS and ATP production are typical indicators for evaluating mitochondrial function. Consistent with expectations, transfection of Flag-PFKFB3 inhibited the decrease in MMP level induced by PA (Fig. S8B, S8D). Furthermore, PFKFB3 overexpression significantly improved the mitochondrial respiratory capacity in PA-treated AC16 cells, characterized by increased basal respiration, ATP-related respiration and maximal respiration (Fig. 6H, I). PFKFB3 overexpression also raised the ATP levels in diabetic myocardium (Fig. 6G). Nonetheless, the knockdown of OPA1 greatly attenuated the beneficial effects of PFKFB3 overexpression on mitochondrial MMP, ATP production, and respiratory function (Figs. 6G–I, S8B, S8D). In conclusion, these results reveal that PFKFB3 overexpression exerts beneficial effects on mitochondrial morphology and function through an OPA1-dependent mechanism in DCM.

PFKFB3 stabilizes OPA1 expression by catalyzing K6-linked polyubiquitination through the E3 ubiquitin ligase NEDD4L

Given the potential effects of OPA1 in PFKFB3 overexpression-mediated inhibitory action against DCM,

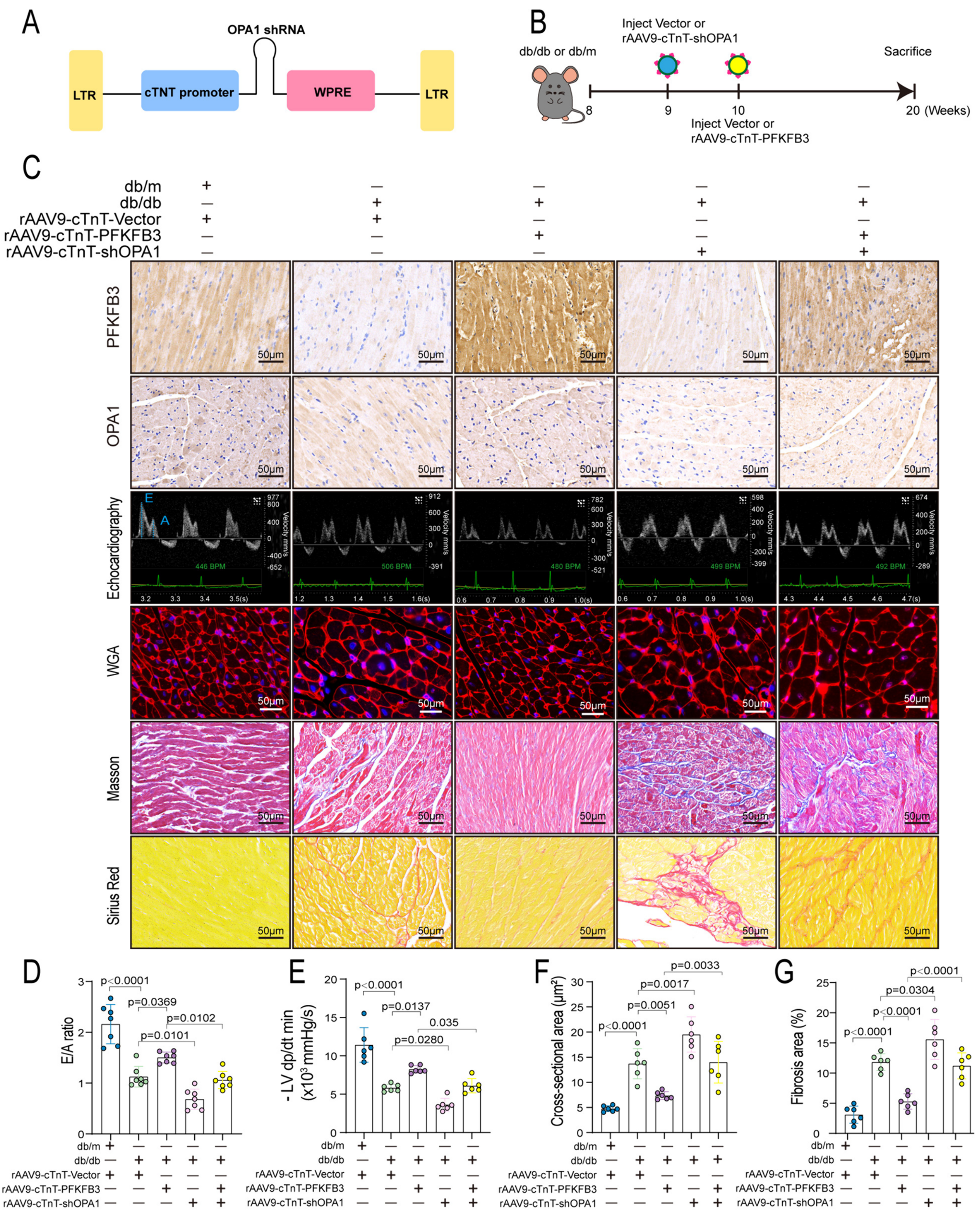
A
OPA1 shRNA
LTR
cTNT promoter
WPRE
LTR
B
db/db or db/m
Inject Vector or rAAV9-cTnT-shOPA1
Sacrifice
8
9
10
20 (Weeks)
Inject Vector or rAAV9-cTnT-PFKFB3
C
db/m + — — — —
db/db — + + + +
rAAV9-cTnT-Vector + + — — —
rAAV9-cTnT-PFKFB3 — — + — +
rAAV9-cTnT-shOPA1 — — — + +
PFKFB3
OPA1
Echocardiography
WGA
Masson
Sirius Red
50μm
E
A
446 BPM
506 BPM
480 BPM
499 BPM
492 BPM
Velocity mm/s
D
E/A ratio
p<0.0001
p=0.0369
p=0.0102
p=0.0101
E
-LV dp/dt min ($\times 10^3$ mmHg/s)
p<0.0001
p=0.0137
0.035
p=0.0280
F
Cross-sectional area (μm^2)
p=0.0033
p=0.0017
p=0.0051
p<0.0001
G
Fibrosis area (%)
p<0.0001
p=0.0304
p<0.0001
p<0.0001
db/m + — — — —
db/db — + + + +
rAAV9-cTnT-Vector + + — — —
rAAV9-cTnT-PFKFB3 — — + — +
rAAV9-cTnT-shOPA1 — — — + +

◂**Fig. 5** OPA1 knockdown attenuated the effects of PFKFB3 overexpression in alleviating cardiac dysfunction and remodeling in db/db mice. **A** Schematic diagram of AAV9-cTnT-shOPA1 structure. **B** Schedule of animal experiments. Nine-week-old mice were injected with rAAV9-cTnT-shOPA1 or vector, and then a week later, mice were injected with rAAV9-cTnT-Flag-PFKFB3 or vector. Finally, mice were sacrificed at the age of 20 weeks. **C** Immunohistochemical staining of PFKFB3 and OPA1 expression. Echocardiography displays the E/A ratio. WGA staining was used to evaluate cardiomyocyte size. Masson staining and Sirius Red staining were used to assess fibrosis. **D** Quantitative analysis of E/A ratio. **E** Haemodynamic analysis of the minimal first derivative of LV pressure (-LV dP/dt min). **F** Quantitative analysis of WGA staining for cross-section area. **G** Quantitative analysis of Masson staining for fibrosis area. n = 6/group. Data are expressed as mean ± SD. $p < 0.05$ was considered significant

we investigated the underlying mechanisms by which PFKFB3 overexpression upregulates OPA1 expression. As shown in Fig. 4K, PFKFB3 overexpression did not affect the OPA1 mRNA level. Therefore, we further explored whether increased OPA1 expression induced by PFKFB3 overexpression was mediated by inhibited degradation at the protein level. We pretreated AC16 cells with Ad-GFP and Ad-PFKFB3, followed by PA treatment for 48 h. Cycloheximide (CHX), a protein synthesis inhibitor, was then added at different time points before harvest. Western blot analysis demonstrated a lower rate of OPA1 degradation in the Ad-PFKFB3 treated cells (Fig. 7A, B). Within eukaryotic cells, two principal mechanisms for protein degradation exist: the autophagy-lysosomal pathway and the ubiquitin-proteasomal pathway. To determine which pathway was involved in OPA1 degradation under PA treatment, we pretreated AC16 cells with Chloroquine (a specific lysosomal inhibitor) and MG132 (a proteasomal inhibitor), either separately or in combination. We used CHX as a positive control in these experiments. Our findings indicated that MG132, either alone or in combination with Chloroquine, significantly blocked the degradation of OPA1 (Fig. 7C and D). The data indicated that PFKFB3 inhibited the degradation of OPA1 via the proteasome pathway.

Modifying a protein with ubiquitin chains is the hallmark of protein degradation by the ubiquitin–proteasome system (UPS). Interestingly, PFKFB3 overexpression increased the endogenous ubiquitination levels of OPA1 (Fig. 7E). To investigate this further, we co-transfected HEK293T cells with plasmids expressing HA-OPA1 and/or Flag-PFKFB3 and/or His-Ubiquitin. The data revealed that PFKFB3 overexpression enhanced the exogenous ubiquitination of OPA1 (Fig. 7F). Posttranslational modification in the form of protein ubiquitination is a dynamic and multifaceted process. When a ubiquitin molecule is attached to a substrate protein through the lysine site of the substrate, there are 7 lysine sites (commonly K6, K11, K27, K29, K33, K48, and K63) and 1 methionine site on the ubiquitin molecule that can be further linked to other ubiquitin molecules. We constructed plasmids containing single-site mutations in ubiquitin to investigate which polyubiquitin chain type is involved in PFKFB3 overexpression-mediated OPA1 ubiquitination. The data demonstrated that PFKFB3 overexpression mediated OPA1 ubiquitination, with only K6R (Lys6-Arg) Ubiquitin completely inhibiting PFKFB3-mediated OPA1 polyubiquitination (Fig. 7G). To further corroborate this finding, we employed K6-only Ubiquitin plasmids (which retains the K6 lysine residue while mutating the other six lysine residues to arginine), K11-only Ubiquitin plasmids, K27-only Ubiquitin plasmids, K29-only Ubiquitin plasmids, K33-only Ubiquitin plasmids, K48-only Ubiquitin plasmids and K63-only Ubiquitin plasmids. HEK293T cells were co-transfected with these mutated ubiquitin plasmids along with HA-OPA1 plasmids, with or without Flag-PFKFB3 plasmids. As shown in Fig. 7H, PFKFB3 predominantly augmented ubiquitination of the K6 type on OPA1. Moreover, we applied wild-type, K6, K6R, and K0 ubiquitin plasmids to verify the type of PFKFB3-mediated ubiquitination (Fig. 7I). Consistent with the previous results, K6-Ubiquitin promoted chain formation on OPA1, similar to wild-type ubiquitin (Fig. 7I). These results revealed that PFKFB3 overexpression stabilized OPA1 protein by promoting its K6-linked polyubiquitination.

The process of ubiquitination involves three enzyme types: ubiquitin-activating enzyme E1, ubiquitin-conjugating enzyme E2, and ubiquitin-protein ligase E3, in which an E3 ubiquitin ligase is substrate-specific. In addition, deubiquitinases are responsible for substrate protein deubiquitination. In this study, we utilized the Ubibrowser website to predict the E3 ubiquitin ligase and deubiquitinase of the OPA1 protein. We compared the predicted top 20 E3 ubiquitin ligase and the only deubiquitinase (CYLD) with the results obtained from IP-MS analysis of OPA1, respectively. Two E3 ubiquitin ligases were filtered out: NEDD4L and smurf1 (Fig. 7J–L). The results of the Co-IP experiment further confirmed the interaction between NEDD4L and OPA1 but not smurf1 (Fig. 7N). HEK293T cells were transfected with HA-OPA1 and cmyc-NEDD4L, with or without Flag-PFKFB3. The Co-IP assays revealed that PFKFB3 overexpression enhanced the interaction between OPA1 and NEDD4L (Fig. 7M). Next, we knocked down NEDD4L using small interference RNA, the sequence of si-2 was selected for further research (Fig. 7O, P). The knockdown of NEDD4L effectively inhibited the PFKFB3-mediated increase in OPA1 expression (Fig. 7Q, R). These results suggest that E3 ligase NEDD4L mediates the ubiquitination of OPA1 facilitated by PFKFB3 overexpression.

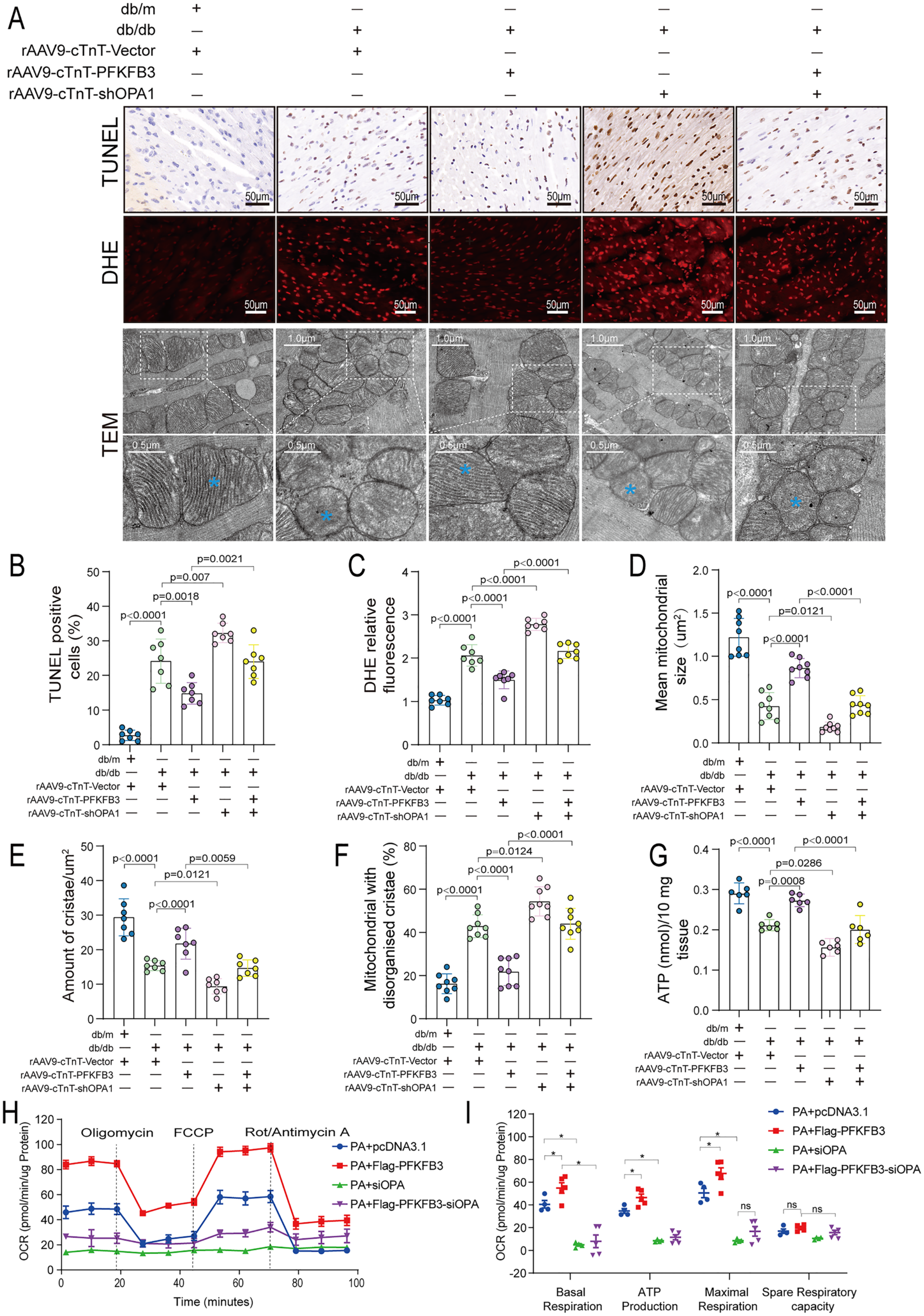
A
db/m + — — — —
db/db — + + + +
rAAV9-cTnT-Vector + + — — —
rAAV9-cTnT-PFKFB3 — — + — +
rAAV9-cTnT-shOPA1 — — — + +
TUNEL
DHE
TEM
50μm
1.0μm
0.5μm
B
TUNEL positive cells (%)
p<0.0001
p=0.0018
p=0.007
p=0.0021
C
DHE relative fluorescence
p<0.0001
p<0.0001
p<0.0001
p<0.0001
D
Mean mitochondrial size (um²)
p<0.0001
p<0.0001
p=0.0121
p<0.0001
E
Amount of cristae/um²
p<0.0001
p<0.0001
p=0.0121
p=0.0059
F
Mitochondrial with disorganised cristae (%)
p<0.0001
p<0.0001
p=0.0124
p<0.0001
G
ATP (nmol)/10 mg tissue
p<0.0001
p=0.0008
p=0.0286
p<0.0001
H
OCR (pmol/min/ug Protein)
Oligomycin
FCCP
Rot/Antimycin A
Time (minutes)
PA+pcDNA3.1
PA+Flag-PFKFB3
PA+siOPA
PA+Flag-PFKFB3-siOPA
I
OCR (pmol/min/ug Protein)
*
ns
Basal Respiration
ATP Production
Maximal Respiration
Spare Respiratory capacity

◂**Fig. 6** OPA1 knockdown attenuated the inhibitory effects of PFKFB3 overexpression on myocardial oxidative stress, apoptosis, mitochondrial fragmentation, and dysfunction in db/db mice. **A** Representative TUNEL staining images (Scale bars, 50 μm), DHE staining microphotographs (Scale bars, 50 μm) and transmission electron microscopic images of mitochondria (Scale bars, 1 μm, 0.5 μm). **B** Quantitative data of the percentage of TUNEL positive cells. **C** Quantitative analysis of DHE relative fluorescence. **D** Quantitative analysis of mean mitochondrial size. **E** Cristae number per μm^2. **F** The proportion of mitochondria with disorganized cristae. **G** Quantification of ATP levels per 10 mg cardiac tissue. n = 6–7/group. **H**, **I** Oxygen consumption rate (OCR) and quantitative statistical analysis of OCR, n = 4/group. Data are expressed as mean ± SD. $p < 0.05$ was considered significant

Discussion

Diabetic cardiomyopathy (DCM) is a prominent cause of death in diabetics [34]. Despite advances in treatment, the prognosis of DCM remains unfavorable. In this study, we explored the distinct role of PFKFB3 overexpression in DCM and revealed several crucial findings: (1) PFKFB3 expression was reduced in the hearts of db/db mice. (2) Cardiac-specific overexpression of PFKFB3 significantly alleviated diabetic cardiac dysfunction and myocardial remodeling, associated with enhanced mitochondrial function and reduced cardiomyocyte apoptosis. (3) The knockdown of OPA1 attenuated the protective effects of PFKFB3 overexpression on diabetic cardiac dysfunction and myocardial remodeling in db/db mice. (4) Mechanistically, PFKFB3 stabilizes OPA1 expression by promoting its K6-linked polyubiquitination mediated by the E3 ligase NEDD4L, thereby preventing the degradation of OPA1 by the ubiquitin–proteasome system. Taken together, cardiac-specific overexpression of PFKFB3 significantly protected against DCM by enhancing myocardial OPA1 stability through NEDD4L-mediated atypical K6-linked polyubiquitination. Our study highlights PFKFB3/OPA1 as promising therapeutic targets for DCM.

The mitochondria serves as the powerhouse for all eukaryotic cells. Maintaining a dynamic balance between mitochondrial fission and fusion is crucial for preserving mitochondrial function. Diabetic hearts exhibit excessive mitochondrial fission and mitochondrial dysfunction characterized by reduced MMP, decreased ATP levels, and impaired OXPHOS, leading to excessive ROS production and apoptosis [35, 36]. Hence, mitochondrial dysfunction is considered a hallmark of DCM [37]. Chen et al. reported that IL-22 mitigated kidney damage by AMPK/AKT signaling and inhibiting mitochondrial dysfunction via PFKFB3 [16]. This study suggests a potential relationship between PFKFB3 and mitochondrial function, but the underlying mechanism remains unclear. In our study, PFKFB3 overexpression inhibited excessive mitochondrial fission and improved mitochondrial function. Mechanistically, PFKFB3 interacts with OPA1 and prevents its degradation in DCM. Hence, targeting PFKFB3/OPA1-mediated enhanced mitochondrial function represents a promising strategy for treating DCM.

The OPA1 gene, located on 3q28, spans over 100 kb and comprises 31 exons [38]. The OPA1 protein is involved in various functions, including promoting mitochondrial fusion, maintaining the respiratory chain [39] and membrane potential [40], organization of cristae, and regulating apoptosis [32]. Previous studies have emphasized the significance of OPA1 in DCM. Liu et al. revealed that paeonol induces OPA1-mediated mitochondrial fusion through the activation of the CK2α-Stat3 pathway in DCM [36]. Ding et al. reported that the mitochondrial fusion promoter-M1 restores mitochondrial dynamics balance and ameliorates DCM, which is dependent on OPA1 [33]. Furthermore, Punicalagin prevents DCM by promoting OPA1-mediated mitochondrial fusion via the PTP1B-Stat3 pathway [36, 41]. To further underscore the beneficial role of OPA1 in diabetic cardiomyopathy, we investigated the effects of OPA1 upregulation on apoptosis and ROS in AC16 cells. AC16 cells were transfected with either pcDNA3.1 or pcDNA3.1-HA-OPA1 plasmids, followed by PA or solvent control treatment. As shown in Fig. S9A–S9F, OPA1 overexpression significantly reduced apoptosis and the ROS production in PA-treated AC16 cells. These studies and our data demonstrate the close association between OPA1 and DCM, underscoring the potential of OPA1 as a promising therapeutic target for DCM.

Ubiquitination, the covalent attachment of ubiquitin to specific substrate proteins, is a multifunctional post-translational modification that affects various disease processes, including cardiovascular disease. Ubiquitination can take various forms, including monoubiquitination, multi-monoubiquitination, and polyubiquitination at specific lysine residues (K6, K11, K27, K29, K33, K48, and K63), as well as at the N-terminal methionine of ubiquitin. K48-linked chains are the predominant and extensively studied type of linkage involved in the degradation of ubiquitinated substrates by the UPS. In this process, substrates tagged with K48-linked chains are recognized, bound, and subsequently degraded by the 26S proteasome. K63-linked ubiquitination is the second most well-known and abundant type, implicated in endocytosis and the innate immune response. Other atypical ubiquitin sites, such as K11-linked ubiquitination, are associated with regulating the cell cycle or earmarking substrates for degradation. However, this type modulates protein–protein interactions or stabilizes proteins such as β-Catenin [42]. The DNA damage response has been repeatedly shown to be controlled by K6-linked ubiquitination [43, 44]. K6 and

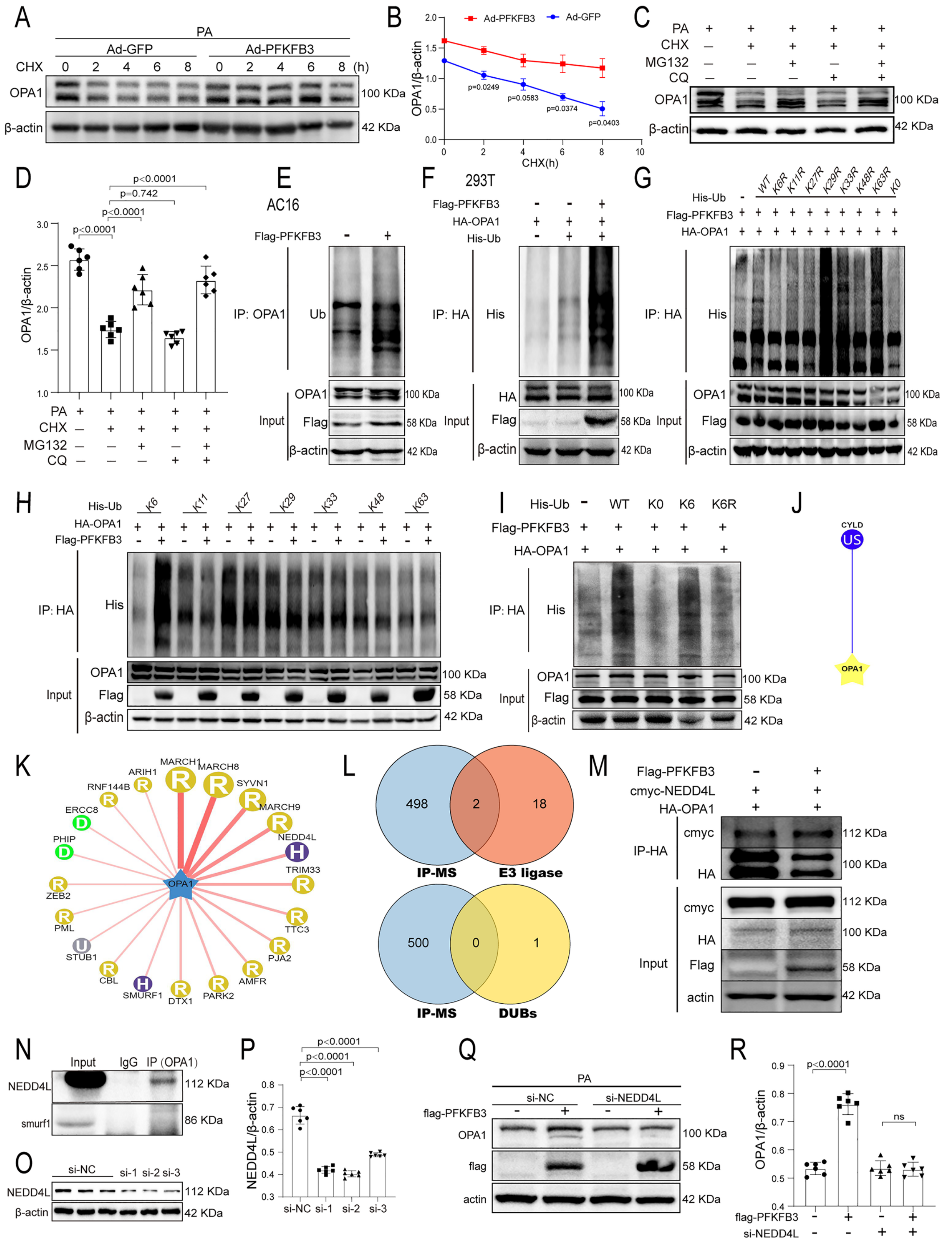
A
PA
Ad-GFP
Ad-PFKFB3
CHX 0 2 4 6 8 0 2 4 6 8 (h)
OPA1
100 KDa
β-actin
42 KDa
B
Ad-PFKFB3
Ad-GFP
OPA1/β-actin
2.0 1.5 1.0 0.5 0.0
0 2 4 6 8 10
CHX(h)
p=0.0249
p=0.0583
p=0.0374
p=0.0403
C
PA + + + + +
CHX – + + + +
MG132 – – + – +
CQ – – – + +
OPA1
100 KDa
β-actin
42 KDa
D
p<0.0001
p=0.742
p<0.0001
p<0.0001
OPA1/β-actin
3.0 2.5 2.0 1.5 1.0
PA + + + + +
CHX – + + + +
MG132 – – + – +
CQ – – – + +
E
AC16
Flag-PFKFB3 - +
IP: OPA1
Ub
Input
OPA1
Flag
β-actin
100 KDa
58 KDa
42 KDa
F
293T
Flag-PFKFB3 - - +
HA-OPA1 + + +
His-Ub - + +
IP: HA
His
Input
HA
Flag
β-actin
100 KDa
58 KDa
42 KDa
G
His-Ub - WT K6R K11R K27R K29R K33R K48R K63R K0
Flag-PFKFB3 + + + + + + + + + +
HA-OPA1 + + + + + + + + + +
IP: HA
His
Input
OPA1
Flag
β-actin
100 KDa
58 KDa
42 KDa
H
His-Ub K6 K11 K27 K29 K33 K48 K63
HA-OPA1 + + + + + + + + + + + + + +
Flag-PFKFB3 - + - + - + - + - + - + - +
IP: HA
His
Input
OPA1
Flag
β-actin
100 KDa
58 KDa
42 KDa
I
His-Ub - WT K0 K6 K6R
Flag-PFKFB3 + + + + +
HA-OPA1 + + + + +
IP: HA
His
Input
OPA1
Flag
β-actin
100 KDa
58 KDa
42 KDa
J
CYLD
US
OPA1
K
MARCH1
MARCH8
ARIH1
SYVN1
RNF144B
MARCH9
ERCC8
NEDD4L
PHIP
TRIM33
ZEB2
OPA1
PML
TTC3
STUB1
PJA2
CBL
AMFR
SMURF1
DTX1
PARK2
L
498 2 18
IP-MS
E3 ligase
500 0 1
IP-MS
DUBs
M
Flag-PFKFB3 - +
cmyc-NEDD4L + +
HA-OPA1 + +
IP-HA
cmyc
HA
112 KDa
100 KDa
Input
cmyc
HA
Flag
actin
112 KDa
100 KDa
58 KDa
42 KDa
N
Input IgG IP (OPA1)
NEDD4L
smurf1
112 KDa
86 KDa
O
si-NC si-1 si-2 si-3
NEDD4L
β-actin
112 KDa
42 KDa
P
p<0.0001
p<0.0001
p<0.0001
NEDD4L/β-actin
0.8 0.7 0.6 0.5 0.4 0.3
si-NC si-1 si-2 si-3
Q
PA
si-NC
si-NEDD4L
flag-PFKFB3 - + - +
OPA1
flag
actin
100 KDa
58 KDa
42 KDa
R
p<0.0001
ns
OPA1/β-actin
0.9 0.8 0.7 0.6 0.5 0.4
flag-PFKFB3 - + - +
si-NEDD4L - - + +

◂**Fig. 7** PFKFB3 stabilizes OPA1 by catalyzing K6-linked polyubiquitination through the E3 ubiquitin ligase NEDD4L. **A**, **B**. Western blot and quantification analysis of OPA1 protein. AC16 cells were pretreated with Ad-PFKFB3 and Ad-GFP for 12 h. Following PA (200 μM) treatment for 48 h, cells were exposed to CHX (cycloheximide, 100 μg/ml) for indicated times before harvest. **C**, **D** Western blot and quantification of OPA1 protein in AC16 cells treated with PA (200 μM) for 48 h. CHX (100 μg/ml), MG132 (proteasome inhibitors, 5 μM), and CQ (chloroquine, autophagy lysosomal inhibitors, 20 μM) were administered for 6 h before harvest. **E** Co-Immunoprecipitation (IP) of AC16 cells transfected with Flag-PFKFB3 plasmids or vectors. **F** Co-IP of HEK293T cells transfected with HA-OPA1, Flag-PFKFB3, and His-ubiquitin plasmids. **G**, **H** Influence of ubiquitin KR (Lys to Arg) mutants (**G**) and K-only ubiquitin mutants (**H**) on PFKFB3-mediated OPA1 polyubiquitination. HEK293T cells were transfected with specified constructs, and OPA1 ubiquitination was assessed. **I** Impact of wild type, K0, K6, and K6R on PFKFB3-mediated OPA1 polyubiquitination. **J**, **K** Identification of top 20 predicted E3 ubiquitin ligases (**K**) and the sole deubiquitinase (CYLD) (**J**) using the Ubibrowser website. **L** Venn diagram illustrating the intersection of IP-MS analysis of OPA1 with predicted E3 ubiquitin ligases and deubiquitinase of the OPA1 protein. **M** Co-IP assay of HA-OPA1 and cmyc-NEDD4L in HEK293T cells, with or without Flag-PFKFB3 presence. **N** Immunoprecipitation using an anti-OPA1 antibody, followed by Western blot analysis with anti-NEDD4L and anti-smurf1 antibody, utilizing cellular extracts from AC16 cells. **O** Assessment of NEDD4L small interfering RNA (siRNA) knockdown efficiency. **P** Quantitative analysis of NEDD4L siRNA transfection efficiency. **Q**, **R** Western blot and quantitative analysis of OPA1 in AC16 cells transfected with either negative control siRNA or NEDD4L siRNA for 6 h, followed by transfection with pcDNA3.1 or Flag-PFKFB3 for 6 h, and finally, PA treatment for 48 h. n = 6/group. Data are expressed as mean ± SD. $p < 0.05$ was considered significant

K63-linked chains play a crucial role in the autophagic processing of damaged mitochondria [45]. K27-linked ubiquitination plays a role in antimicrobial, antiviral immunity, and antifungal signaling [46]. The joint presence of K27 and K29-linked chains has been reported to promote proteasomal and autophagic degradation and protein aggregation associated with Parkinson's disease [47, 48]. In our study, PFKFB3 overexpression stabilized OPA1 by promoting its K6-linked polyubiquitination mediated by the E3 ligase NEDD4L, thereby suppressing mitochondrial fragmentation and restoring mitochondrial function in db/db mice.

The mechanism by which PFKFB3 overexpression reduces ROS production in DCM may be multifaceted. On one hand, PFKFB3 mitigates oxidative stress in cardiac tissues of diabetic mice by interacting with OPA1 and inhibiting the downregulation of OPA1 expression, which leads to a reduction in oxidative stress. Chen et al. reported that the decrease in OPA1 expression resulted in increased levels of ROS [49]. We found that PFKFB3 could stabilize OPA1 expression, thereby reducing ROS production. On the other hand, PFKFB3 overexpression may alleviate oxidative stress by stimulating glycolysis. Previous studies have indicated that promoting glycolysis resulted in reduced oxygen consumption and ROS production [50]. In this study, when glycolysis was inhibited by 2-DG, the production of ROS increased (Fig. S5G). Hence, PFKFB3 may mitigate the generation of ROS by modulating both OPA1 and glycolytic pathways.

It is important to acknowledge that our study has certain limitations. Firstly, OPA1 predominantly exists at the mitochondrial membrane, while PFKFB3 is situated in the cytoplasm and nucleus, prompting a compelling question: How do they interact? Previous studies have reported that OPA1 is encoded by a nuclear gene, implying that the translational process of OPA1 occurs in the cytoplasmic ribosome [51]. Additionally, Kar et al. discovered that newly synthesized forms of OPA1 undergo ubiquitination [52]. In our study, PFKFB3 mediated the ubiquitination of OPA1. Consequently, we hypothesize that upon OPA1 synthesis in the cytoplasm, PFKFB3 interacts with OPA1 and recruits the E3 ubiquitin ligase NEDD4L, which mediates ubiquitination of OPA1, thereby escorting OPA1 from the cytosol to the mitochondria and protecting it from degradation by the proteasome. Nevertheless, the precise mechanisms require further clarification. Secondly, the db/db mice and AC16 cells used in our study may not entirely replicate the pathophysiology of patients with DCM. Thirdly, additional investigation is required to ascertain whether the protective benefits of PFKFB3 can be extended to other diabetic models, including female mice. Despite these limitations, our study provides valuable insights into the role of PFKFB3 in mitigating DCM.

Conclusion

Cardiac-specific overexpression of PFKFB3 protects against DCM by enhancing myocardial OPA1 stability via NEDD4L-mediated atypical K6-linked polyubiquitination. Our findings imply that PFKFB3/OPA1 might be therapeutic targets for DCM.

Supplementary information

Extended information about the Materials and Methods and Supplementary Figures can be accessed in the Supplementary Materials.

Supplementary Information The online version contains supplementary material available at https://doi.org/10.1007/s00018-024-05257-5.

Acknowledgements The authors appreciate Dr. Cong-Yi Wang, Dr. Ting Wang, and Dr. Xi Luo from the Center for Biomedical Research of Tongji Hospital for kindly providing the Seahorse XFe24 Analyzer and technical assistance.

Authors' contributions All authors contributed to the study conception and design. Material preparation, data collection and analysis were performed by Jinlan Luo, Shuiqing Hu, Jingrui Liu, Lili Shi, Liman Luo, Wenhua Li, Yueting Cai, Jiaxin Tang, Siyang Liu, Menglu Fu, Ruolan Dong, Yan Yang. The first draft of the manuscript was written by Jinlan Luo and all authors commented on previous versions of the manuscript. All authors read and approved the final manuscript.

Funding This work was supported by the National Natural Science Foundation of China (No. 82070825, No. 81873512, and No. 82004254) and the National Key Research and Development Program of China (Grant No. 2020YFC2008905).

Data availability The datasets generated during and/or analysed during the current study are available from the corresponding author on reasonable request.

Declarations

Conflict of interests The authors have no relevant financial or non-financial interests to disclose.

Ethical approval This study was performed in line with the principles of the Declaration of Helsinki. Approval was granted by the Experimental Animal Research Committee of Tongji Medical College, Huazhong University of Science and Technology (IACUC Issue No.: TJH-202109019). Our studies strictly adhered to the Guidelines from Directive 2010/63 EU of the European Parliament and ARRIVE guidelines.

Consent for publication All authors agree to the publication of this study.

Open Access This article is licensed under a Creative Commons Attribution 4.0 International License, which permits use, sharing, adaptation, distribution and reproduction in any medium or format, as long as you give appropriate credit to the original author(s) and the source, provide a link to the Creative Commons licence, and indicate if changes were made. The images or other third party material in this article are included in the article's Creative Commons licence, unless indicated otherwise in a credit line to the material. If material is not included in the article's Creative Commons licence and your intended use is not permitted by statutory regulation or exceeds the permitted use, you will need to obtain permission directly from the copyright holder. To view a copy of this licence, visit http://creativecommons.org/licenses/by/4.0/.

References

1. Diabetes is a pandemic of unprecedented magnitude now affecting one in 10 adults worldwide. Diabetes Res Clin Pract. 2021; 181: 109133
2. Knapp M, Tu X, Wu R (2019) Vascular endothelial dysfunction, a major mediator in diabetic cardiomyopathy. Acta Pharmacol Sin 40(1):1–8
3. Rubler S, Dlugash J, Yuceoglu YZ, Kumral T, Branwood AW, Grishman A (1972) New type of cardiomyopathy associated with diabetic glomerulosclerosis. Am J Cardiol 30(6):595–602
4. Ritchie RH, Abel ED (2020) Basic mechanisms of diabetic heart disease. Circ Res 126(11):1501–1525
5. Zhang Q, Li D, Dong X, Zhang X, Liu J, Peng L et al (2022) LncDACH1 promotes mitochondrial oxidative stress of cardiomyocytes by interacting with sirtuin3 and aggravates diabetic cardiomyopathy. Sci China Life Sci 65(6):1198–1212
6. Furtado RHM, Bonaca MP, Raz I, Zelniker TA, Mosenzon O, Cahn A et al (2019) Dapagliflozin and cardiovascular outcomes in patients with type 2 diabetes mellitus and previous myocardial infarction. Circulation 139(22):2516–2527
7. Bethel MA, Patel RA, Merrill P, Lokhnygina Y, Buse JB, Mentz RJ et al (2018) Cardiovascular outcomes with glucagon-like peptide-1 receptor agonists in patients with type 2 diabetes: a meta-analysis. Lancet Diabetes Endocrinol 6(2):105–113
8. Pop-Busui R, Januzzi JL, Bruemmer D, Butalia S, Green JB, Horton WB et al (2022) Heart failure: an underappreciated complication of diabetes a consensus report of the American Diabetes Association. Diabetes Care 45(7):1670–1690
9. Kim J-A, Wei Y, Sowers JR (2008) Role of mitochondrial dysfunction in insulin resistance. Circ Res 102(4):401–414
10. Shadel GS, Horvath TL (2015) Mitochondrial ROS signaling in organismal homeostasis. Cell 163(3):560–569
11. Dillmann WH (2019) Diabetic cardiomyopathy: what is it and can it be fixed? Circ Res 124(8):1160–1162
12. Bock FJ, Tait SWG (2020) Mitochondria as multifaceted regulators of cell death. Nat Rev Mol Cell Biol 21(2):85–100
13. He Y, Zhou L, Fan Z, Liu S, Fang W (2018) Palmitic acid, but not high-glucose, induced myocardial apoptosis is alleviated by N-acetylcysteine due to attenuated mitochondrial-derived ROS accumulation-induced endoplasmic reticulum stress. Cell Death Dis 9(5):568
14. Huynh K, Kiriazis H, Du X-J, Love JE, Jandeleit-Dahm KA, Forbes JM et al (2012) Coenzyme Q10 attenuates diastolic dysfunction, cardiomyocyte hypertrophy and cardiac fibrosis in the db/db mouse model of type 2 diabetes. Diabetologia 55(5):1544–1553
15. Zeng H, Pan T, Zhan M, Hailiwu R, Liu B, Yang H et al (2022) Suppression of PFKFB3-driven glycolysis restrains endothelial-to-mesenchymal transition and fibrotic response. Signal Transduct Target Ther 7(1):303
16. Chen W, Shen Y, Fan J, Zeng X, Zhang X, Luan J et al (2021) IL-22-mediated renal metabolic reprogramming via PFKFB3 to treat kidney injury. Clin Transl Med 11(2):e324
17. Yi M, Ban Y, Tan Y, Xiong W, Li G, Xiang B (2019) 6-Phosphofructo-2-kinase/fructose-2,6-biphosphatase 3 and 4: a pair of valves for fine-tuning of glucose metabolism in human cancer. Mol Metab 20:1–13
18. Guo R, Wu Z, Jiang J, Liu C, Wu B, Li X et al (2017) New mechanism of lipotoxicity in diabetic cardiomyopathy: deficiency of Endogenous H2S Production and ER stress. Mech Ageing Dev 162:46–52
19. Li C, Liu Z, Xu Q, Peng H, Cao J, Zhou H et al (2021) PXDN reduces autophagic flux in insulin-resistant cardiomyocytes via modulating FoxO1. Cell Death Dis 12(5):418
20. Prasad K-MR, Xu Y, Yang Z, Acton ST, French BA (2011) Robust cardiomyocyte-specific gene expression following systemic injection of AAV: in vivo gene delivery follows a Poisson distribution. Gene Ther 18(1):43–52
21. Li H, Yang Q, Huang Z, Liang C, Zhang D-H, Shi H-T et al (2022) Dual-specificity phosphatase 12 attenuates oxidative stress injury and apoptosis in diabetic cardiomyopathy via the ASK1-JNK/p38 signaling pathway. Free Radic Biol Med 192:13–24
22. Zhang B, Li X, Liu G, Zhang C, Zhang X, Shen Q et al (2021) Peroxiredomin-4 ameliorates lipotoxicity-induced oxidative stress and apoptosis in diabetic cardiomyopathy. Biomed Pharmacother 141:111780

23. Chistiakov DA, Shkurat TP, Melnichenko AA, Grechko AV, Orekhov AN (2018) The role of mitochondrial dysfunction in cardiovascular disease: a brief review. Ann Med 50(2):121–127
24. Xue W, Cai L, Tan Y, Thistlethwaite P, Kang YJ, Li X et al (2010) Cardiac-specific overexpression of HIF-1α prevents deterioration of glycolytic pathway and cardiac remodeling in streptozotocin-induced diabetic mice. Am J Pathol 177(1):97–105
25. Gu J, Wang S, Guo H, Tan Y, Liang Y, Feng A et al (2018) Inhibition of p53 prevents diabetic cardiomyopathy by preventing early-stage apoptosis and cell senescence, reduced glycolysis, and impaired angiogenesis. Cell Death Dis 9(2):82
26. Zhong L, Li J, Yu J, Cao X, Du J, Liang L et al (2024) Anemarrhena asphodeloides Bunge total saponins ameliorate diabetic cardiomyopathy by modifying the PI3K/AKT/HIF-1α pathway to restore glycolytic metabolism. J Ethnopharmacol 319(Pt 3):117250
27. Li L, Zeng H, He X, Chen J-X (2021) Sirtuin 3 alleviates diabetic cardiomyopathy by regulating TIGAR and cardiomyocyte metabolism. J Am Heart Assoc 10(5):e018913
28. Alvarez R, Mandal D, Chittiboina P (2021) Canonical and non-canonical roles of PFKFB3 in brain tumors. Cells 10(11):2913
29. Cantelmo AR, Conradi L-C, Brajic A, Goveia J, Kalucka J, Pircher A et al (2016) Inhibition of the glycolytic activator PFKFB3 in endothelium induces tumor vessel normalization, impairs metastasis, and improves chemotherapy. Cancer Cell 30(6):968–985
30. Jia W, Zhao X, Zhao L, Yan H, Li J, Yang H et al (2018) Non-canonical roles of PFKFB3 in regulation of cell cycle through binding to CDK4. Oncogene 37(13):1685–1698
31. Fu R-H (2023) Pectolinarigenin improves oxidative stress and apoptosis in mouse NSC-34 motor neuron cell lines induced by C9-ALS-associated proline-arginine dipeptide repeat proteins by enhancing mitochondrial fusion mediated via the SIRT3/OPA1 axis. Antioxidants (Basel). 12(11):2008
32. Frezza C, Cipolat S, Martins de Brito O, Micaroni M, Beznoussenko GV, Rudka T et al (2006) OPA1 controls apoptotic cristae remodeling independently from mitochondrial fusion. Cell 126(1):177–189
33. Ding M, Liu C, Shi R, Yu M, Zeng K, Kang J et al (2020) Mitochondrial fusion promoter restores mitochondrial dynamics balance and ameliorates diabetic cardiomyopathy in an optic atrophy 1-dependent way. Acta Physiol (Oxf) 229(1):e13428
34. Hu S, Luo J, Guo P, Du T, Liu X, He M et al (2023) Lentinan alleviates diabetic cardiomyopathy by suppressing CAV1/SDHA-regulated mitochondrial dysfunction. Biomed Pharmacother 167:115645
35. Cai C, Wu F, He J, Zhang Y, Shi N, Peng X et al (2022) Mitochondrial quality control in diabetic cardiomyopathy: from molecular mechanisms to therapeutic strategies. Int J Biol Sci 18(14):5276–5290
36. Liu C, Han Y, Gu X, Li M, Du Y, Feng N et al (2021) Paeonol promotes Opa1-mediated mitochondrial fusion via activating the CK2α-Stat3 pathway in diabetic cardiomyopathy. Redox Biol 46:102098
37. Chang X, Li Y, Cai C, Wu F, He J, Zhang Y et al (2022) Mitochondrial quality control mechanisms as molecular targets in diabetic heart. Metabolism 137:155313
38. Lenaers G, Reynier P, Elachouri G, Soukkarieh C, Olichon A, Belenguer P et al (2009) OPA1 functions in mitochondria and dysfunctions in optic nerve. Int J Biochem Cell Biol 41(10):1866–1874
39. Varanita T, Soriano ME, Romanello V, Zaglia T, Quintana-Cabrera R, Semenzato M et al (2015) The OPA1-dependent mitochondrial cristae remodeling pathway controls atrophic, apoptotic, and ischemic tissue damage. Cell Metab 21(6):834–844
40. Olichon A, Baricault L, Gas N, Guillou E, Valette A, Belenguer P et al (2003) Loss of OPA1 perturbates the mitochondrial inner membrane structure and integrity, leading to cytochrome c release and apoptosis. J Biol Chem 278(10):7743–7746
41. Fu F, Liu C, Shi R, Li M, Zhang M, Du Y et al (2021) Punicalagin protects against diabetic cardiomyopathy by promoting opa1-mediated mitochondrial fusion via regulating PTP1B-Stat3 pathway. Antioxid Redox Signal 35(8):618–641
42. Li Z, Wang Y, Li Y, Yin W, Mo L, Qian X et al (2018) Ube2s stabilizes β-Catenin through K11-linked polyubiquitination to promote mesendoderm specification and colorectal cancer development. Cell Death Dis 9(5):456
43. Elia AEH, Boardman AP, Wang DC, Huttlin EL, Everley RA, Dephoure N et al (2015) Quantitative proteomic atlas of ubiquitination and acetylation in the DNA damage response. Mol Cell 59(5):867–881
44. Wu-Baer F, Lagrazon K, Yuan W, Baer R (2003) The BRCA1/BARD1 heterodimer assembles polyubiquitin chains through an unconventional linkage involving lysine residue K6 of ubiquitin. J Biol Chem 278(37):34743–34746
45. Ordureau A, Heo J-M, Duda DM, Paulo JA, Olszewski JL, Yanishevski D et al (2015) Defining roles of PARKIN and ubiquitin phosphorylation by PINK1 in mitochondrial quality control using a ubiquitin replacement strategy. Proc Natl Acad Sci U S A 112(21):6637–6642
46. Cao Z, Conway KL, Heath RJ, Rush JS, Leshchiner ES, Ramirez-Ortez ZG et al (2015) The ubiquitin ligase TRIM62 regulates CARD9-mediated anti-fungal immunity and intestinal inflammation. Immunity 43(4):715–726
47. Nazio F, Carinci M, Valacca C, Bielli P, Strappazzon F, Antonioli M et al (2016) Fine-tuning of ULK1 mRNA and protein levels is required for autophagy oscillation. J Cell Biol 215(6):841–856
48. He X, Zhu Y, Zhang Y, Geng Y, Gong J, Geng J et al (2019) RNF34 functions in immunity and selective mitophagy by targeting MAVS for autophagic degradation. EMBO J 38(14):e100978
49. Le C, Liu T, Tran A, Lu X, Tomilov AA, Davies V et al (2012) OPA1 mutation and late-onset cardiomyopathy: mitochondrial dysfunction and mtDNA instability. J Am Heart Assoc 1(5):003012
50. Zhou D, Shao L, Spitz DR (2014) Reactive oxygen species in normal and tumor stem cells. Adv Cancer Res 122:1–67
51. Rocatcher A, Desquiret-Dumas V, Charif M, Ferré M, Gohier P, Mirebeau-Prunier D et al (2023) The top 10 most frequently involved genes in hereditary optic neuropathies in 2186 probands. Brain 146(2):455–460
52. Kar R, Mishra N, Singha PK, Venkatachalam MA, Saikumar P (2010) Mitochondrial remodeling following fission inhibition by 15d-PGJ2 involves molecular changes in mitochondrial fusion protein OPA1. Biochem Biophys Res Commun 399(4):548–554

Publisher's Note Springer Nature remains neutral with regard to jurisdictional claims in published maps and institutional affiliations.